Optimizing reproductive success of corals spawned in land-based nurseries

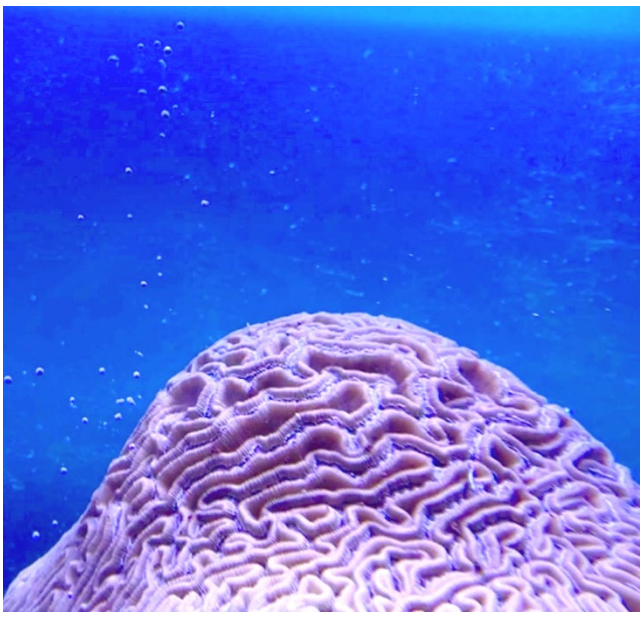

Diploria labyrinthiformis colony spawning, May 2025

Optimizing reproductive success of corals spawned in land-based nurseries

Final Report

Prepared By:

Nicole Fogarty

Ashley Weeks

Krista Laforest

Danielle Norton

Kerri Dobson

University of North Carolina Wilmington Coral REEF Lab

June 15, 2025

Completed in Fulfillment of C4012C for

Florida Department of Environmental Protection
Coral Protection and Restoration Program
8000 N Ocean Dr.
Dania Beach, FL 33004

This report should be cited as follows:
Fogarty, ND, Laforest, KV, Weeks, A, Norton, D, Dobson, KL. 2025. Optimizing reproductive success of corals spawned in land-based nurseries. Florida Department of Environmental Protection, 1-43.

This report was prepared for the Florida Department of Environmental Protection's (DEP) Coral Protection and Restoration Program by UNCW REEF Lab. Funding was provided by the DEP Award No. C4012C. The views, statements, findings, conclusions, and recommendations expressed herein are those of the authors and do not necessarily reflect the views of the State of Florida or any of its sub-agencies.

Management Summary

The UNCW Coral REEF Lab continues to advance applied research focused on improving the success of ex situ coral spawning, larval care, and early life-stage growth and survivorship to support restoration efforts. Over the past year, we have successfully spawned an additional coral species, *Diploria labyrinthiformis*, expanded our analysis of coral sperm traits to better understand fertilization dynamics, and researched ways to increase settlement and recruit growth and survival. We conducted color-based settlement experiments with *Pseudodiploria clivosa* and *Orbicella faveolata* to inform larval habitat preferences and enhance settlement success. Our work on microbial probiotics has progressed with *P. clivosa* recruits, identifying a promising group of bacterial strains that may enhance survivorship and growth in the species. Additionally, we have compiled a regional calendar of coral spawning patterns for Florida, which will support the planning and coordination of spawning-based restoration activities. These efforts contribute directly to optimizing land-based coral propagation and increasing the efficiency of reef restoration interventions.

Executive Summary

Florida's Coral Reef is experiencing a multi-year disease-related mortality event, in addition to increased frequency and severity of thermal stress events, resulting in massive die-offs in multiple coral species. Collection of corals for gene banks and sexual coral reproduction efforts is being utilized to help protect genetic diversity and restore coral reefs in Florida. The logistical difficulties of collecting coral gametes in the field and transporting them to a laboratory for fertilization within a one-hour time window have limited utility for research in reproductive ecology. Additionally rearing larvae and settling corals in a field setting without adequate controls of light and temperature has limited the number and health of coral recruits produced for restoration. Innovative and radical measures are needed to assist with the recovery of Florida's Coral Reef. Sexual reproduction is critical to coral recovery by increasing genetic diversity and creating individuals that are potentially resistant to the factors that have led to coral mortality. Coral fertilization, larval development, and recruitment are the most vulnerable life history stages, and are therefore the most important for our understanding of coral reef resilience. Among the suggested transformative research endeavors is land-based coral spawning, assisted fertilization, settlement, and subsequent rearing for experimentation and restoration. The main objective of this research is to improve the methods of ex situ coral sexual propagation, with the aim of increasing genetic diversity of corals and upscaling restoration techniques. This was primarily accomplished through two research areas: (1) enhancing methods in ex situ coral spawning, fertilization, and larval and recruit rearing, and (2) developing probiotics for coral early life-history stages. This year, we successfully induced spawning in an additional species, *Diploria labyrinthiformis,* with 9 out of the 13 maintained colonies releasing gametes. We also determined that purple ceramic tiles result in higher survival of *O. faveolata* recruits compared to white and grey ceramic tiles. Finally, several probiotic strains were found to enhance the survival and growth of *Pseudodiploria clivosa* recruits. These findings have furthered our knowledge and understanding of various aspects of ex situ sexual reproduction and recruit grow-out techniques to upscale restoration efforts and enhance the genetic diversity of wild populations in the coming years.

Acknowledgements

We thank the Florida Department of Environmental Protection for their continued financial support of these projects, UNCW's Center for Marine Science (CMS) for providing the infrastructure for conducting this research, and aquaculture specialists Jimmy White and Ron Moore for their assistance. Furthermore, we thank Kory Enneking for the original construction and Louis-Pierre Rich for the construction during the expansion of our facility and the facilitation of several research projects. Additionally, we would like to thank Dr. Ushijima and his laboratory for their assistance with bacterial isolation and identification. This research could not have been completed without the dedication of the following UNCW students: Meg Van Horn, Alexandra Zelaya, Anna Edmundson, Avry Regan, Diego Fabian, Emily Heubel, Gabrielle Deighton, Grace Purcell, Hailey Grabinsky, Joseph Bilotta, Kayleen Bello, Lahna McCann, Lindsey Campbell, Madison Harper, Mazzy Morrison, Megan Burke, Paige Shackelford, Samantha Paul, Tyler Pratt, and Victoria Lesslie. Finally, we thank the CMS leadership and staff for the continued support of our coral spawning facility.

TABLE OF CONTENTS

List of Figures

List of Tables

List of Acronyms

MAS	Minutes after sunset
DAFM	Days after full moon
GLMM	Generalized linear mixed model

1. AQUARIUM-BASED CORAL SEXUAL REPRODUCTION

1.1. Overview

Efforts to maintain and spawn corals in the land-based nursery at UNCW continued over the past year. As this technology has only been applied to Caribbean corals relatively recently, the methodologies and infrastructure are continually optimized to maximize spawning success and recruit survival. This year we again shifted spawning time by 4 hours. Gametes were collected, fertilized, and reared in larval cones, flat-bottom bins, and dish bins lined with mesh before being exposed to pre-conditioned tiles with CCA dust collected off Broward County. A pilot study was conducted with colored ceramic tiles to determine whether certain colors may improve settlement.

For the past two years, we have worked to establish the best practices in collecting sperm traits for the purpose of understanding individual broodstock sperm viability, how sperm will perform under future climate scenarios, and if sperm morphology and swimming traits vary among species. However, we have been limited by the available technology.

All recruits produced from ex situ spawning were grown in dedicated raceways and received continual care and supplemental feedings. This has broad implications for ex situ coral reproduction and will help inform managers and stakeholders on how to optimize facility design and spawning protocols for upscaling restoration activities. Dr. Fogarty continued to coordinate and facilitate the land-based assisted sexual reproduction (LASR) group consisting of experts in artificial light and indoor spawning cue mimics. This group shares valuable information on land-based spawning techniques that advance knowledge in this emerging field. The LASR group met in person at the December 2024 Reef Futures meeting. In May 2025, LASR leaders held a Question and Answer Session for members of facilities that are establishing or are interested in establishing land-based spawning systems.

1.2. Methods

1.2.1. Spawning and fertilization

All coral colonies housed within the lab for spawning originated from Broward County. *Orbicella faveolata* (n = 11), *Pseudodiploria clivosa* (n = 15), and *Acropora cervicornis* (n = 11) were added to our system between 2020–2021 and thus have been held ex-situ in our facility for 3–4 years. *Diploria labyrinthiformis* colonies (n = 13) were collected and added to the system in June 2024. Our ex situ system mimics seasonal conditions experienced by corals in Broward County by altering temperature and light (solar and lunar) cycles. The species housed within our facility have been identified as rescue

priorities in the State of Florida, while *Acropora cervicornis* is critically endangered. Colonies of *A. cervicornis* and *P. clivosa* were monitored for spawning in July, with the addition of *O. faveolata* in August and September 2024. *Diploria labyrinthiformis* was monitored for spawning in April – June 2025.

In preparation for spawning season each year, sunset time was shifted to occur 4 hours earlier in the day to facilitate research efforts and prevent researcher fatigue. We implement best practices to reduce all potential light pollution in the spawning cubicles (e.g., taping over equipment lights in cubicles and closing curtains before sunset). We are continuing to maintain the best husbandry practices in all broodstock systems (e.g., daily monitoring of water quality, regular water changes, and feeding 3x weekly). We have been working on maximizing feeding in our spawning systems while simultaneously maintaining water quality (i.e., limiting phosphates and slightly increasing nitrates) to ensure the best possible coral health and growth. Currently, we are feeding smaller amounts of less viscous food mixture three times per week, which is more than double the amount what we have fed in the past.

During the spawning window for May-June, spawning was monitored 3.5 hours prior to sunset until 90 minutes after sunset. During each spawning window in July-September, monitoring for spawning activity began three days after the full moon (DAFM), 90 minutes after sunset (MAS). Colonies were initially monitored every 10 minutes until setting occurred, after which the corals were continuously monitored until spawning commenced. During spawning, the coral species, tag ID, time of colony setting, proportion of colony setting, and spawn time were recorded. Once gamete bundles from a colony reached the surface, they were collected via pipette or petri dish. Bundles were then added to a gravy separator or, in the case of a smaller spawn ($n < 200$ bundles), small cups. Bundles from multiple colonies (ideally >3) were then mixed in equal portions and gently swirled for approximately 90 minutes to encourage the bundles to break apart. To optimize fertilization opportunities, sperm concentrations were targeted at 10^6 sperm/ml by keeping a ratio of approximately 1 gamete bundle to 1 ml of seawater. Gravy separators were then placed in 27.5 ºC water baths for 1–2 hours until the first cell cleavage occurred. Embryos were then rinsed a minimum of five times with clean seawater to avoid polyspermy.

In early 2025, we set up our larval rearing bin system in anticipation of *D. labyrinthiformis* spawning, with some minor adjustments to the inflow lines and drainage systems in some of the bins to better accommodate species that require more water flow.

1.2.2. Sperm Morphology and Motility

We have partnered with a local IVF clinic, Wilmington Fertility Center, to learn the best practices for measuring sperm motility and have gained valuable insight into assessing

sperm for deformations using a specialized staining technique. Additionally, we have been in discussion with researchers who specialize in assessing sperm motility and velocity. With this knowledge, we analyzed photos and videos from the three *Orbicella faveolata* and six *Pseudodiploria clivosa* colonies that spawned in August. Our partners from Wilmington Fertility Center toured our facility earlier this year.

We were able to successfully record videos for sperm velocity and motility during August 2024 spawning. Over three nights we collected data for three *O. faveolata* and six *P. clivosa* colonies, allowing us to examine how sperm motility and quality (i.e., normal and abnormal sperm, head and tail sizes, motility) varies across individuals and between species. However, due to restraints with the OpenCASA Software, we were unable to consistently detect sperm movement, preventing us from accurately assessing sperm velocity. Leveraging university resources, we have upgraded to using CEROS II package and CASA software, which will allow us to accurately detect sperm motility and quantify sperm velocity for future spawning seasons. Our partners at Wilmington Fertility Center have offered to continue to meet with us to advance our understanding of sperm fitness.

To measure sperm traits, labeled Eppendorf tubes of sperm were held in a dry bath to maintain optimal temperature (27.7 °C). 4 µL of diluted sperm (~6.67×10^4 cells mL^{-1}) was placed in a disposable hemacytometer and viewed under 40x magnification using phase contrast on an Olympus IX73 inverted microscope. Using Cellsens software, a minimum of six photos per spawning colony were captured to assess sperm quality. In each photo, an individual sperm was categorized as having normal or abnormal morphology, including discrepancies in sperm head (i.e., free head) and sperm tail (i.e., bent, coiled, tail droplets, shortened, or disconnected tail). Sperm were also analyzed using Cellsens software to measure tail length and sperm head size (HS) using the following equation:

$$HS = (\text{wider diameter} + \text{smaller diameter})/2$$

Morphological differences, in both head and tail size, between colonies was analyzed using a Kruskal Wallis test. A non-parametric one-tailed Mann-Whitney Wilcoxon test was utilized to determine whether there are morphological differences between *P. clivosa* and *O. faveolata* sperm.

To assess motility, a minimum of six, 10-second videos were recorded under 40x magnification using phase contrast on an Olympus IX73 inverted microscope. Videos were then visually assessed to determine the percent motility of sperm. Motility differences between colonies was analyzed using a Kruskal Wallis test. A non-parametric two-tailed Mann-Whitney Wilcoxon test was utilized to determine whether there are differences in motility between *P. clivosa* and *O. faveolata* sperm.

1.2.3. Larval rearing and settlement

In 2024, we used our new larval rearing system. The system includes eight 10-gallon flat-bottom bins with recirculating water via an inflow drip line to the top of each bin from a shared sump outfitted with a UV sterilizer. Insulation, foam lids, and flow rate valves were added to regulate and maintain temperature in each bin.

Between 6,000–10,000 larvae were added to 15 settlement dish bins and 20,000–25,000 remained in the flatbottom larval bin. The bottom of all bins were lined with white and pink tiles and CCA dust. The tiles were scored for settlement (attached but not metamorphosed) or metamorphosed recruits 4–5 days later. To calculate settlement, a subset of 10 tiles from the 34–51 tiles per bin was scored from each of the settlement bin. The average number of recruits of those 10 tiles was used to extrapolate the number of recruits in the bin based on the number of tiles lining the bottom. The average settlement was estimated based on the total number of recruits per bin and the number of larvae added.

1.2.4. No choice settlement experiment with *O. faveolata*

In no-choice settlement experiments, *O. faveolata* larvae (n = 200) were exposed to 15 pink, white, purple, or gray ceramic tiles. Each color treatment was replicated three times. Settlement was assessed 1.5 weeks post-spawning. Survival and growth (temporal changes in total surface area) were measured with AI technology called the COral Area Sizing Tool (COAST) at 2-, 4-, 6-, and 8-weeks post-settlement.

To assess differences in larval settlement across tile colors, we fitted a generalized linear mixed model (GLMM) with a Poisson distribution. Tile color was included as a fixed effect and replicate was included as a random effect. Standard model diagnostics (e.g., residuals, collinearity, outliers, homogeneity of variance, normality of random effects) were verified for each selected model. Estimated marginal means and pairwise comparisons between treatments were calculated, with a Tukey adjustment applied to control for multiple tests.

Survival across tile color treatments was compared using the Mantel-Haenszel (log-rank) test. Kaplan-Meier survival estimates were generated to model survival, and overall differences in survival curves among treatments were assessed with a chi-squared test. Post-hoc pairwise comparisons were conducted using pairwise log-rank tests with Bonferroni-adjusted *p*-values to control for multiple comparisons.

To assess the effects of tile color and time on coral recruit growth, a linear mixed-effects model was fitted to log transformed data (to improve model convergence and meet model assumptions). Tile color and time were included as fixed effects, and recruit ID was included as a random intercept to account for repeated measurements over time. The model was fitted using restricted maximum likelihood (REML), and t-tests with

Satterthwaite's approximation were used to assess fixed effects. Residual diagnostics included graphical assessment of residual distribution via histograms and residual vs. fitted value plots, and a Shapiro-Wilk test for normality. No major deviations from normality or heteroscedasticity were detected, supporting the validity of model assumptions. All statistical analyses were conducted in R (version 4.4.2) within RStudio.

1.2.5. Choice settlement experiment with *P. clivosa*

In choice settlement experiments, larvae of *Pseudodiploria clivosa* (n = 75) were placed in bins containing two differently colored ceramic tiles. A fully factorial design was used to test all combinations of pink, white, purple, and gray ceramic tiles, with six replicates per treatment. Settlement was assessed one week after spawning. Survival and growth (temporal changes in total surface area) were measured with AI technology called the COral Area Sizing Tool (COAST) at 2-, 4-, 6-, and 8-weeks post-settlement.

Settlement data were analyzed using a generalized linear mixed-effects model (GLMM) with a Poisson distribution. Tile color was included as a fixed effect and bin ID was included as a random effect. Models were fitted using maximum likelihood estimation with Laplace approximation and model assumptions were checked by inspecting scaled residuals and testing for overdispersion.

Survival across tile color treatments was compared using the Mantel-Haenszel (log-rank) test. Kaplan-Meier survival estimates were generated to model survival, and overall differences in survival curves among treatments were assessed with a chi-squared test.

To assess the effects of tile color and time on coral recruit growth, a linear mixed-effects model was fitted to log transformed data (to improve model convergence and meet model assumptions). Tile color and time were included as fixed effects, and recruit ID was included as a random intercept to account for repeated measurements over time. The model was fitted using restricted maximum likelihood (REML), and t-tests with Satterthwaite's approximation were used to assess fixed effects. Residual diagnostics included graphical assessment of residual distribution via histograms and residual vs. fitted value plots, and a Shapiro-Wilk test for normality. No major deviations from normality or heteroscedasticity were detected, supporting the validity of model assumptions. All statistical analyses were conducted in R (version 4.4.2) within RStudio.

1.3. Results

1.3.1. Spawning and fertilization

Thus far in spring 2025, 9 out of our 13 *D. labyrinthiformis* colonies successfully spawned (Table 1). In April, evidence of spawning occurred 13 days after the full moon, likely from one colony (Fig. 1). In May, two colonies spawned 9 days after the full moon and 7 colonies spawned the 11 days after the full moon, and 12 colonies spawned the

following day (Fig. 1). Although synchronous, these spawning events occurred between 1200hrs and 1300hrs (374 to 12 minutes before sunset), two hours earlier than expected based on the predicted peak time. We are working to determine why this might be but speculate that this may have occurred due to the abrupt stop in water flow from turning off the tank powerheads to begin spawn watch.

From these 2025 spawning events, 300,000 *D. labyrinthiformis* embryos were produced between these two days of spawning in May, resulting in approximately 189,000 larvae. 20,000 were shared with collaborators at Boston University. The average settlement and metamorphosed were 1.5% and 5.7% respectively, with the overall settlement and metamorphosed 7.2%. This is likely an underrepresentation of recruitment because at this early stage newly metamorphosed corals are difficult to locate, particularly on the pink tiles.

In 2024, spawning only occurred after the August 19th full moon. For *P. clivosa,* 8 of 13 coral colonies spawned (Table 1). As with previous years, spawning occurred mostly on night 8, 1 spawned on night 9, and 2 dribbled on night 10. For *O. faveolata*, 5 of 9 coral colonies spawned (Table 1). Spawning occurred on night 8 for most *O. faveolata* colonies, except for one colony that spawned on night 9. For both species, spawning times after sunset were similar to previous years and those documented in the wild (Figures 2–3). This year, the proportion of the colony releasing gamete bundles and the quality of the gamete bundles (smaller, sank) was lower than previous years.

From these 2024 spawning events, 300,000 *O. faveolata* and >150,000 *P. clivosa* embryos were produced. Of those larvae, 20,000 *O. faveolata* larvae and gametes were provided to NOAA collaborators in South Carolina. Additionally, 10,000 *O. faveolata* and 8,000 *P. clivosa* were provided to on-site collaborators at UNCW. The remaining larvae were retained for use in larval settlement experiments and to grow out for additional experiments and outplanting.

Table 1. *Number of putative genotypes for broodstock (Orbicella faveolata, Pseudodiploria clivosa, Acropora cervicornis, and Diploria labyrinthiformis) that successfully spawned each year. ^ denotes colonies that were in our system for <3 months and * denotes colonies that were diseased or recovering from tissue recession.*

Species	**2020**	**2021**	**2022**	**2023**	**2024**	**2025**
O. faveolata	3 / 4^	3 / 11*^	4 / 11*	7 / 10	5 / 9*	TBD
P. clivosa	4 / 6^	12 / 15^	7 / 15	13 / 15	8 / 13	TBD
A. cervicornis	N/A	4 / 11	4 / 11	2? / 11	0 / 11*	TBD
D. labyrinthiformis	N/A	N/A	N/A	N/A	N/A	9 / 13

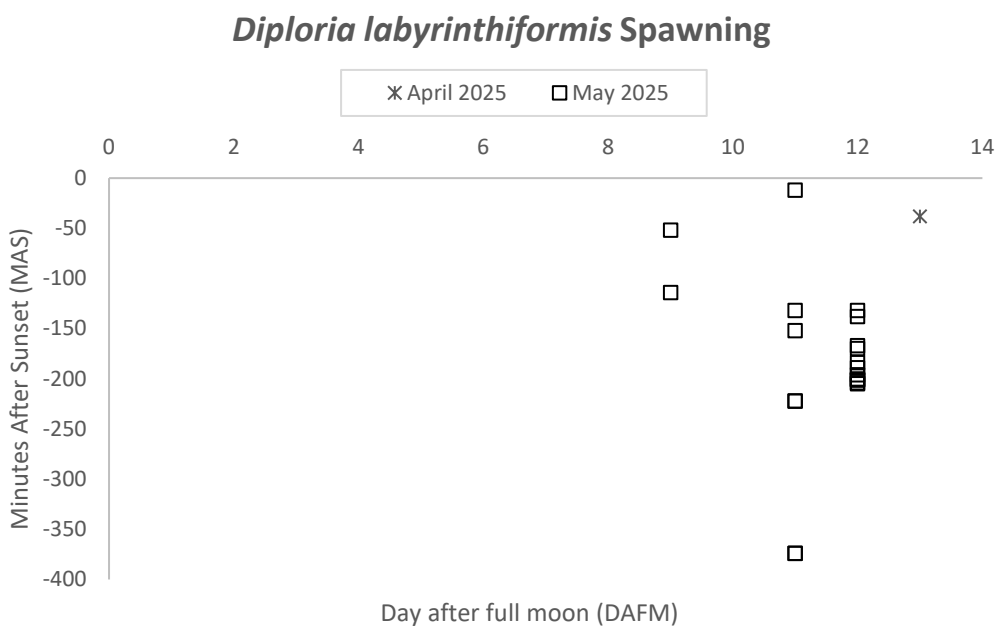

Figure 1. Diploria labyrinthiformis ex situ spawning times in minutes after sunset (MAS) and days after the full moon (DAFM) in April and May 2025, June 2025 will also be monitored.

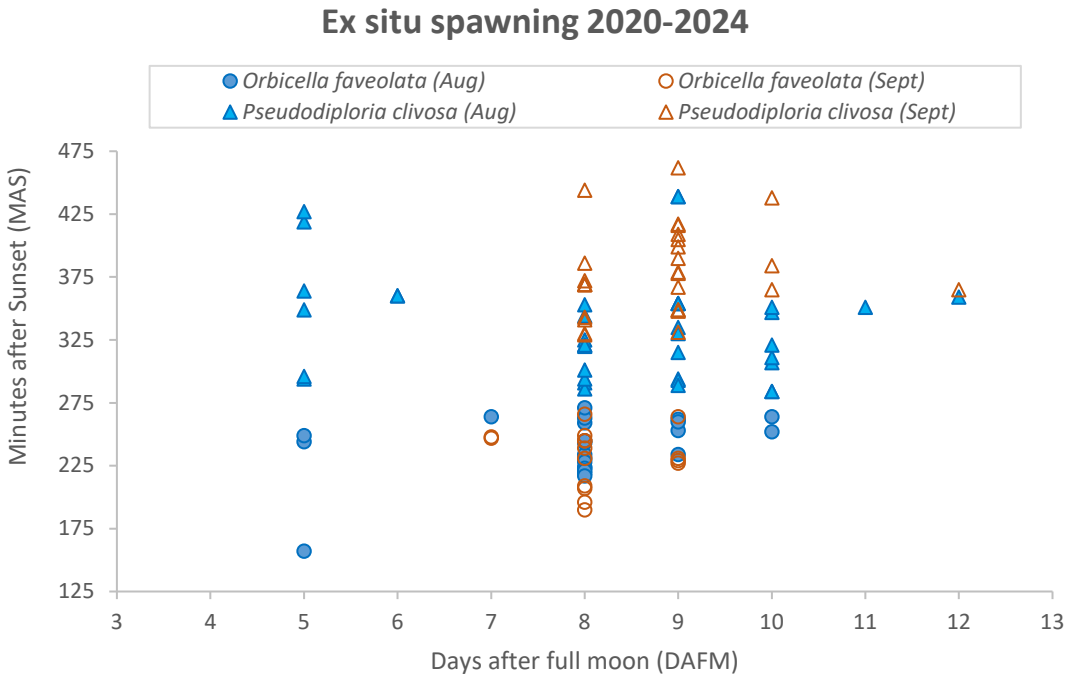

Figure 2 *Ex situ spawning times for Orbicella faveolata (circles) and Pseudodiploria clivosa (triangles) for August (filled) and September (open) at the UNCW facility from 2020–2024.*

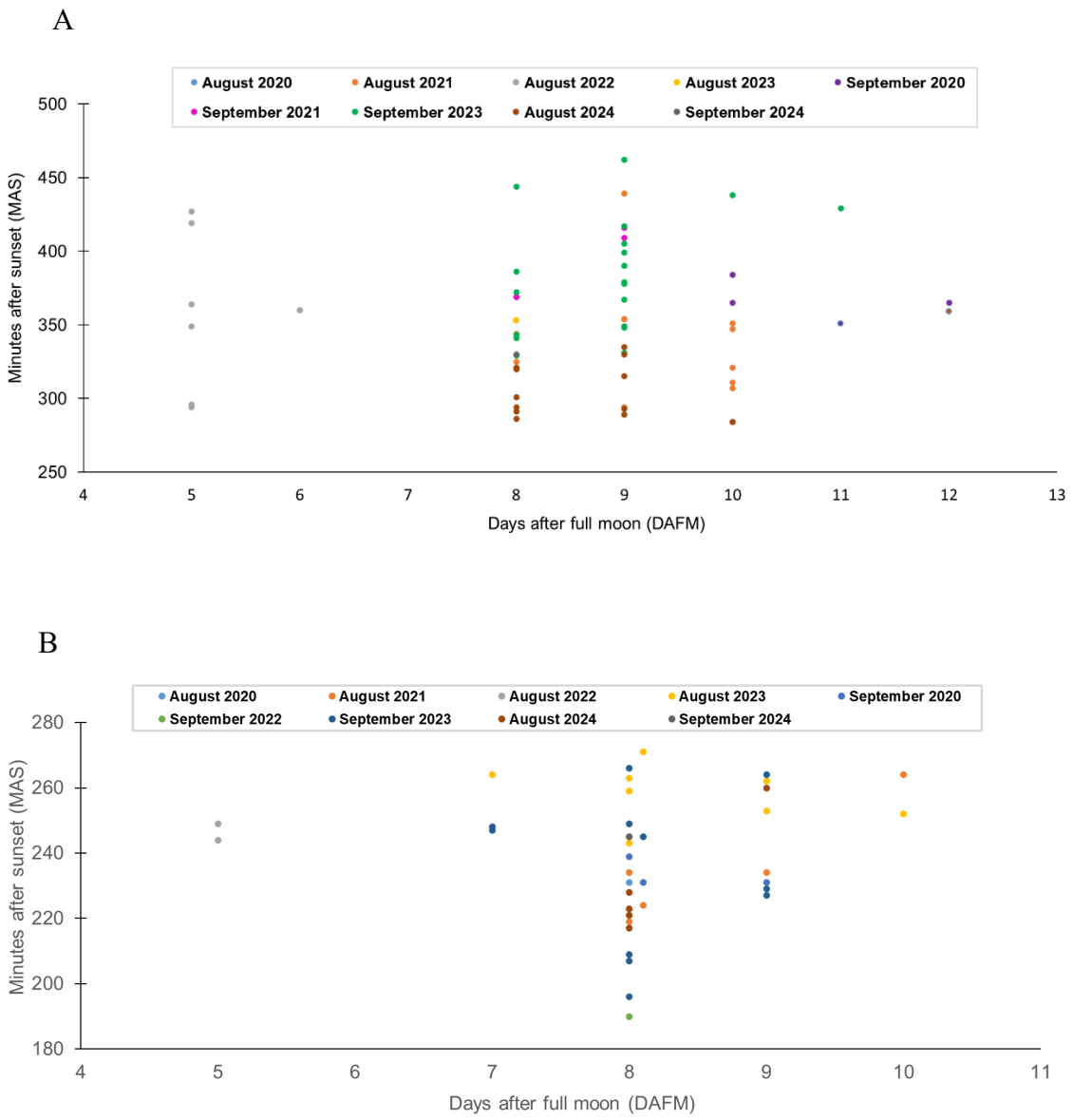

Figure 3. *(A) Pseudodiploria clivosa and (B) Orbicella faveolata spawning times in minutes after sunset (MAS) and days after the full moon (DAFM) in August and September from 2020–2024.*

1.3.2. Sperm Morphology and Motility

The average *O. faveolata* sperm head size was 403.60 ± 75.12 µm (n = 110) and ranged from 280.48–614.88µm. There were no significant differences in head size between individual colonies of *O. faveolata* (Fig. 4A; chi-sq = 0.1552, df = 3, p = 0.9845). The

average *O. faveolata* sperm tail length was 5494.85 ± 1046.47 µm (n = 110) and ranged from 2377.51–6915.82µm. There were significant differences in tail length between individual colonies of *O. faveolata* (Fig. 4B; chi-sq = 21.803, df = 3, $p < 0.0001$). Specifically, OFAV_001 has significantly shorter tails than OFAV_012 and OFAV_013 ($p < 0.05$). Similarly, OFAV_007 has significantly shorter tails than OFAV_012 ($p < 0.05$). The average motility of *O. faveolata* sperm tail length was 87 ± 12 % and ranged from 57–100% motility. There were significant differences in motility between individual colonies of *O. faveolata* (Fig. 5; chi-sq = 35.88553, df = 3, $p < 0.0001$). Specifically, OFAV_001 has significantly lower motility than OFAV_007 and OFAV_012 ($p < 0.05$).

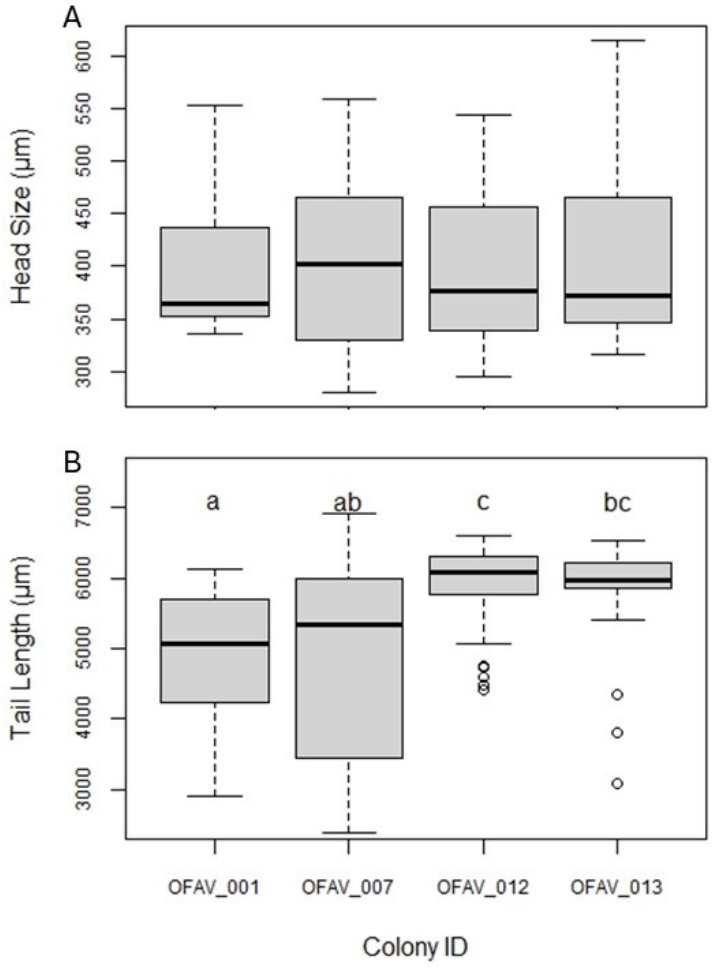

Figure 4*. Average (± SE) A) sperm head size and B) tail size of Orbicella faveolata. Letters indicate significant differences.*

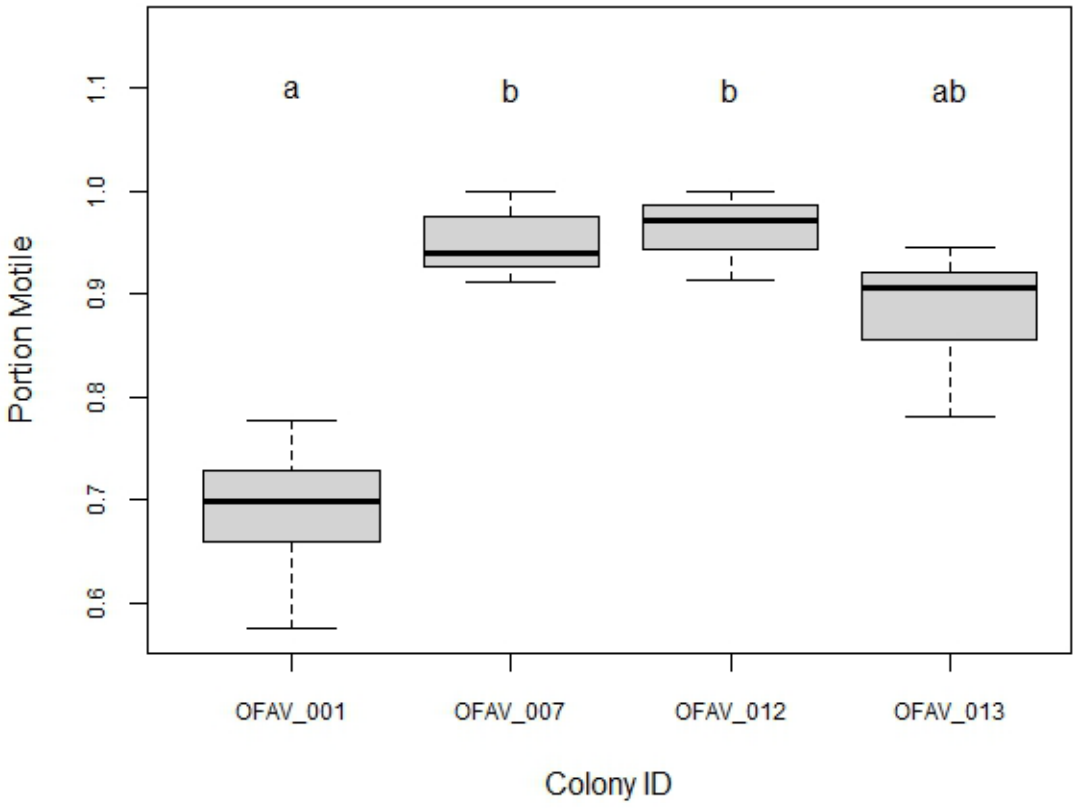

***Figure 5**. Average (± SE) proportion of sperm motility of Orbicella faveolata colonies. Letters indicate significant differences.*

The average *Pseudodiploria clivosa* sperm head size was 324.02 ± 85.62 µm (n = 130) and ranged from 168.00–600.86 µm. There were no significant differences in head size between individual colonies of *P. clivosa* (Fig. 6A; chi-sq = 7.4706, df = 4, $p = 0.113$). The average *P. clivosa* sperm tail length was 3425.92 ± 1176.98 µm (n = 69) and ranged from 763.4–5220.01 µm. There were significant differences in tail length between individual colonies of *P. clivosa* (Fig. 6B; chi-sq = 15.922, df = 4, $p < 0.01$). Specifically, PCLI_004 and PCLI_015 have significantly shorter tails than PCLI_002 ($p < 0.05$). The average motility of *P. clivosa* sperm tail length was 92 ± 8 % and ranged from 69–115% motility. There were significant differences in motility between individual colonies of *P. clivosa* (Fig. 7; chi-sq = 30.13742, df = 4, $p < 0.0001$). Specifically, PCLI_004 has significantly lower motility than PCLI_002, PCLI_011, and PCLI_015 ($p < 0.05$).

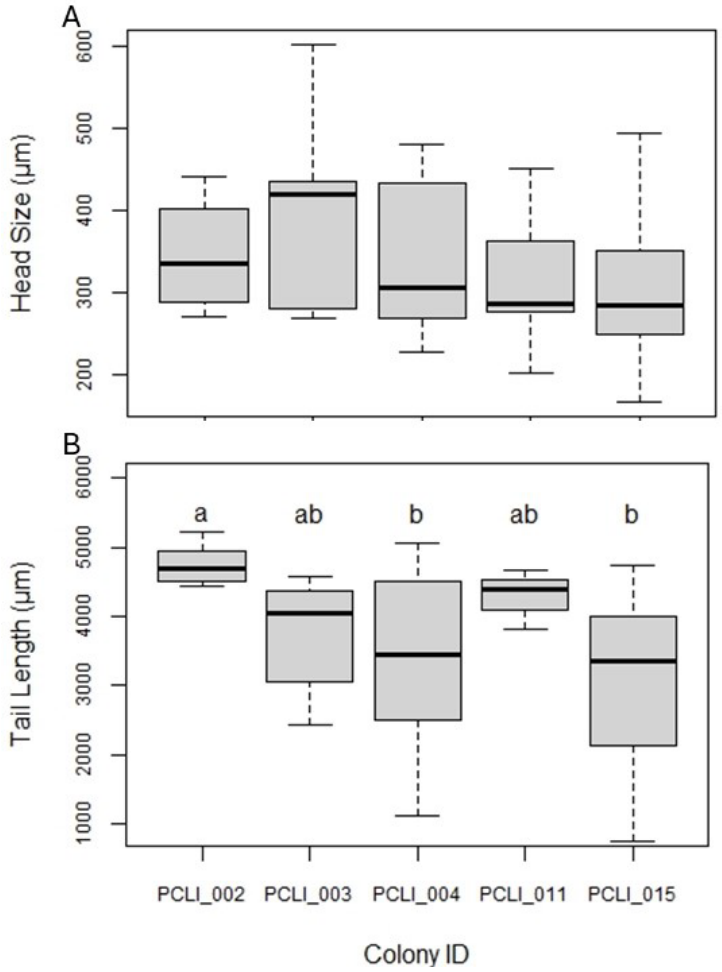

***Fig. 6**. Average (± SE) A) sperm head size and B) tail size of Pseudodiploria clivosa. Letters indicate significant differences.*

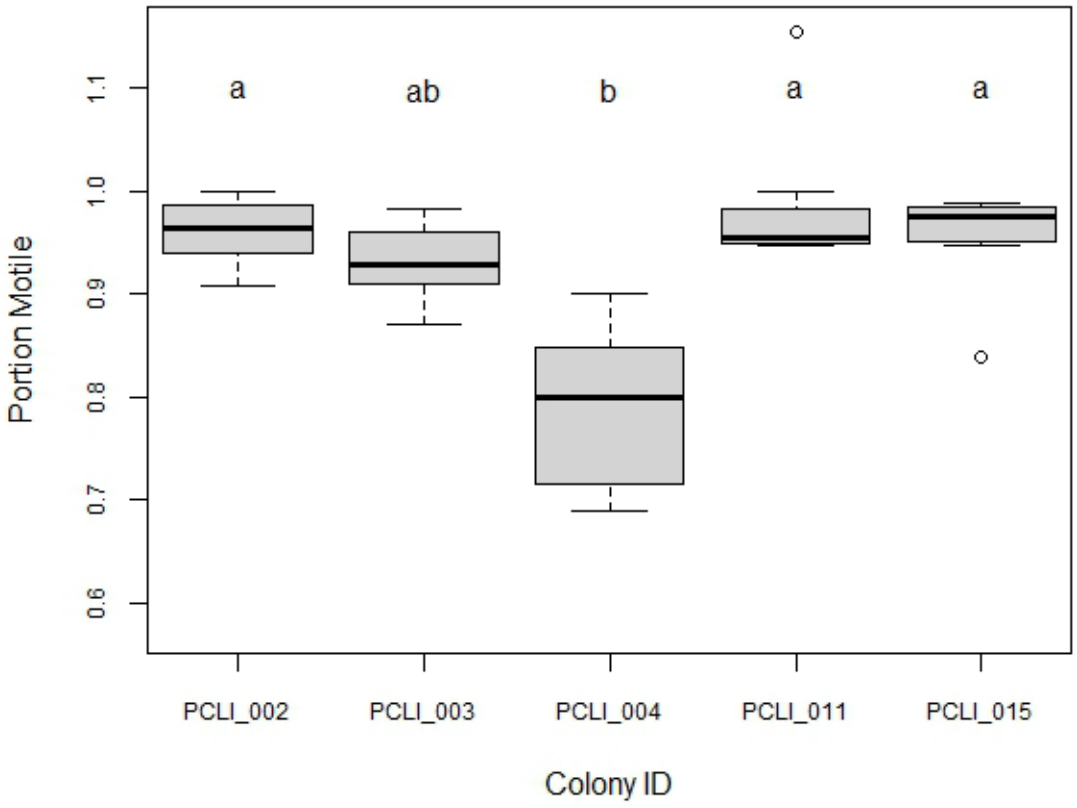

***Figure** 7. Average (± SE) proportion of sperm motility of Pseudodiploria clivosa colonies. Letters indicate significant differences.*

There were significant differences between *O. faveolata* and *P. clivosa* in sperm size, but not shape. Specifically, *O. faveolata* have significantly larger sperm heads (Fig. 8A; W = 8899, $p < 0.0001$) and longer sperm tails (Fig. 8B; W = 8899, $p < 0.0001$) than *P. clivosa.* Moreover, motility between species was marginally insignificant (Fig. 9; W = 1011.5, $p = 0.05684$).

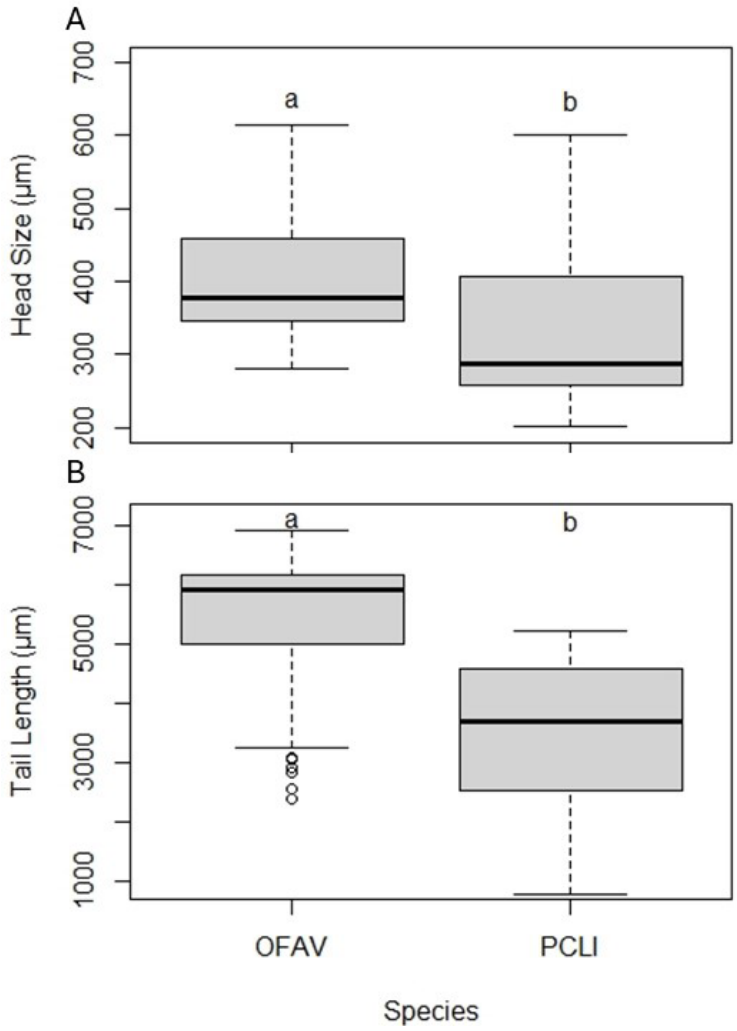

Figure 8. *Average (± SE) A) sperm head size and B) tail size of Orbicella faveolata and Pseudodiploria clivosa. Letters indicate significant differences.*

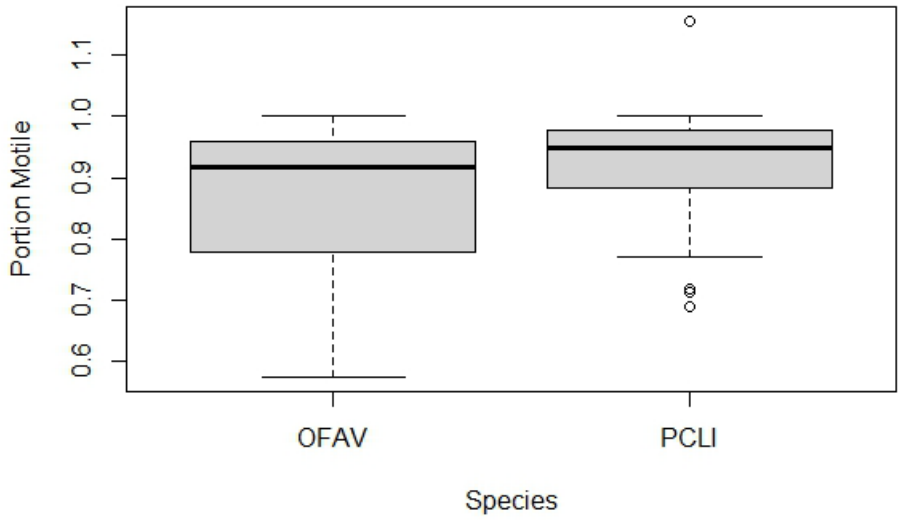

***Figure 9**. Average (± SE) proportion of sperm motility between Orbicella faveolata and Pseudodiploria clivosa.*

Through our partnership with a local IVF clinic, Wilmington Fertility Center, we learned common morphological abnormalities found in sperm. Based on human sperm traits, for a sample to be considered "healthy" there should be 4–14% of sperm with normal morphology, with the latter end being necessary to maximize morphology. *Orbicella faveolata* samples had 71.17% normal sperm morphology. Common abnormalities included bent tails (75% of abnormalities), cytoplasmic droplets (18.8%), and free heads or tails (6.3%). There were no significant differences between head size (chi-sq = 0.12167, df = 1, $p = 0.7272$) nor tail length (chi-sq = 0.41108, df = 1, $p = 0.5214$) between normal and abnormal *O. faveolata* sperm. *Pseudodiploria clivosa* samples had a lower percentage of normal sperm (61.1%), however this was still in the acceptable range for fertilization. Common abnormalities included free heads or tails (57.1% of abnormalities), bent tails (20.6%), cytoplasmic and tail droplets (10.9%), coiled tails (9.5%), and free tails (1.6%). Unlike *O. faveolata,* there were significant differences between tail length in *P. clivosa* sperm (chi-sq = 4.6784, df = 1, $p < 0.05$), with normal tails being significantly longer than abnormal tails. Sperm head size in normal sperm was larger than head size in abnormal sperm, however this was marginally insignificant (chi-sq = 2.9747, df = 1, $p = 0.085$).

1.3.3. Larvae Rearing and Settlement

The 2024 spawning season resulted in 240 *O. faveolata* recruits and 36 *P. clivosa* recruits (Table 2). The 2025 spawning of *D. labyrinthiformis* resulted in 9,586 settled recruits (Table 2).

Table 2. *Current number of coral recruits alive by year and species. * Indicates corals settled from donated larvae from Florida partners.*

Species	**2021**	**2022**	**2023**	**2024**	**2025**
Orbicella faveolata	NA	NA	8	240	TBD
Pseudodiploria clivosa	182	291	226	36	TBD
Pseudodiploria strigosa	NA	NA	142*	NA	TBD
Acropora cervicornis	NA	NA	3*	NA	TBD
Colpophyllia natans	NA	NA	43*	NA	TBD
Montastrea cavernosa	NA	NA	NA	570*	TBD
Diploria labyrinthiformis	NA	NA	NA	NA	9,586

1.3.4. No choice settlement experiment with *O. faveolata*

Orbicella faveolata settlement differed by tile color (Fig. 10). Treatments with white and grey tiles had similarly high settlement (2.42 ± 0.37 larvae per tile and 2.37 ± 0.36 larvae per tile, respectively) and did not differ significantly (ratio = 1.02, $p = 0.9997$). Settlement in bins with pink tiles (1.25 ± 0.22 larvae per tile) was significantly lower than in treatments with white (ratio = 1.93, $p = 0.0251$) and grey tiles (ratio = 1.90, $p = 0.0311$). Treatments with purple tiles had intermediate settlement (2.11 ± 0.33 larvae per tile) that was not significantly different from white (ratio = 1.14, $p = 0.9242$) or grey (ratio = 1.12, $p = 0.9502$) tiles, nor was the difference between purple and pink significant (ratio = 0.59, $p = 0.1128$).

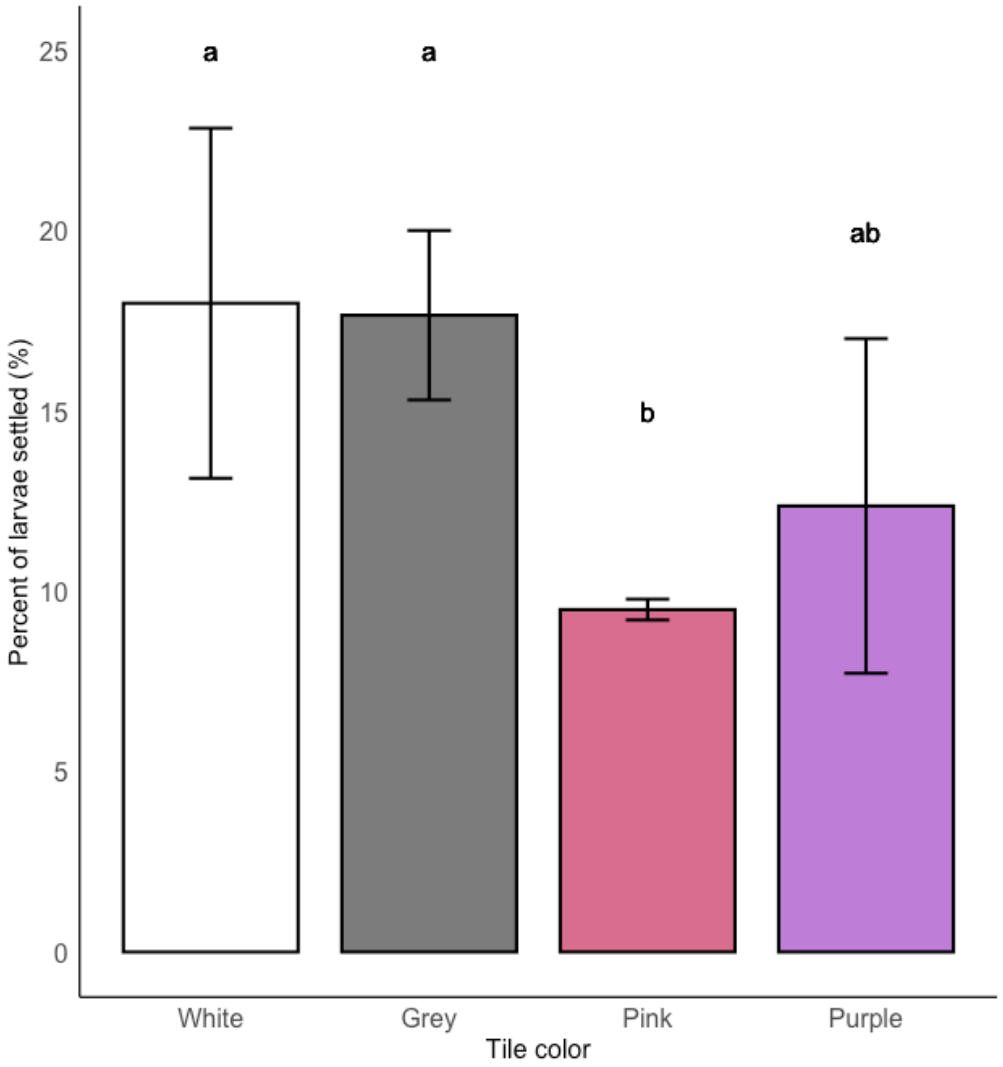

Figure 10. *Average (± SE) percent of Orbicella faveolata larvae settled (of the 200 added) per bin across the four tile colors (n = 3). Letters indicate significant differences.*

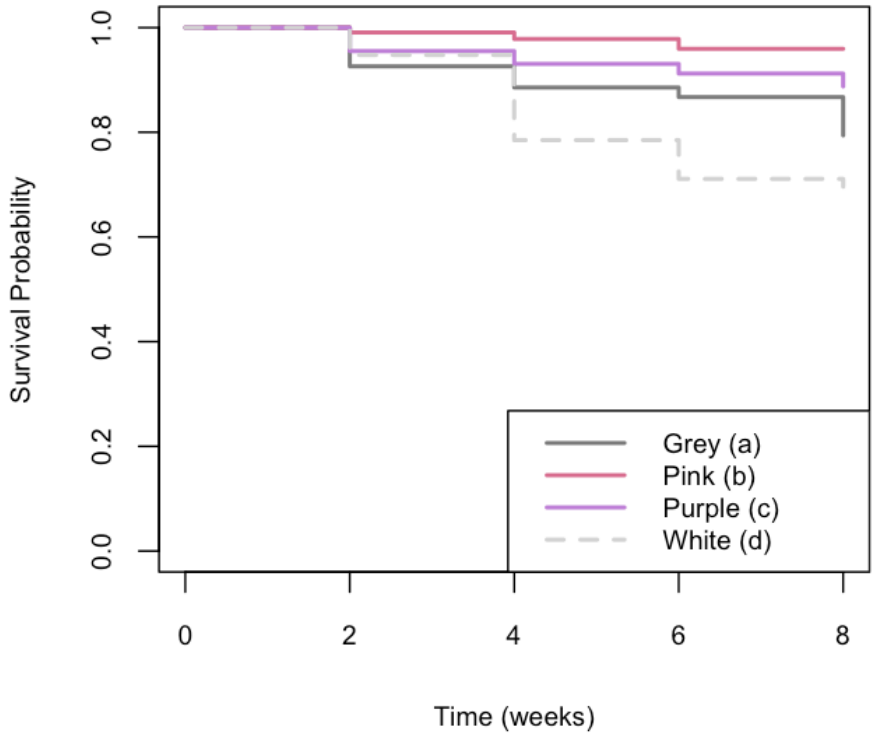

Figure 11. *Probability of survival (Kaplan-Meier survival curves) for Orbicella faveolata over time (2-, 4-, 6-, and 8-weeks post-settlement) by tile color (white, grey, pink, and purple). Lines represent survival probability over time. Letters in parentheses indicate significant differences between tile colors based on pairwise log-rank tests ($p < 0.05$). Treatments sharing different letters are significantly different.*

There were significant differences in *O. faveolata* recruit survivorship across tile color treatment (Mansel-Haenzsel log-rank Survival Analysis, chi-sq = 47.1, df = 3, $p < 0.0001$; Fig. 11). Pairwise comparisons using post-hoc log-rank tests indicated that all color groups differed significantly from each other ($p < 0.05$); recruits on white tiles had significantly lower survival probability compared to all other tile colors, while those on pink tiles had the highest survival probability (Fig. 11).

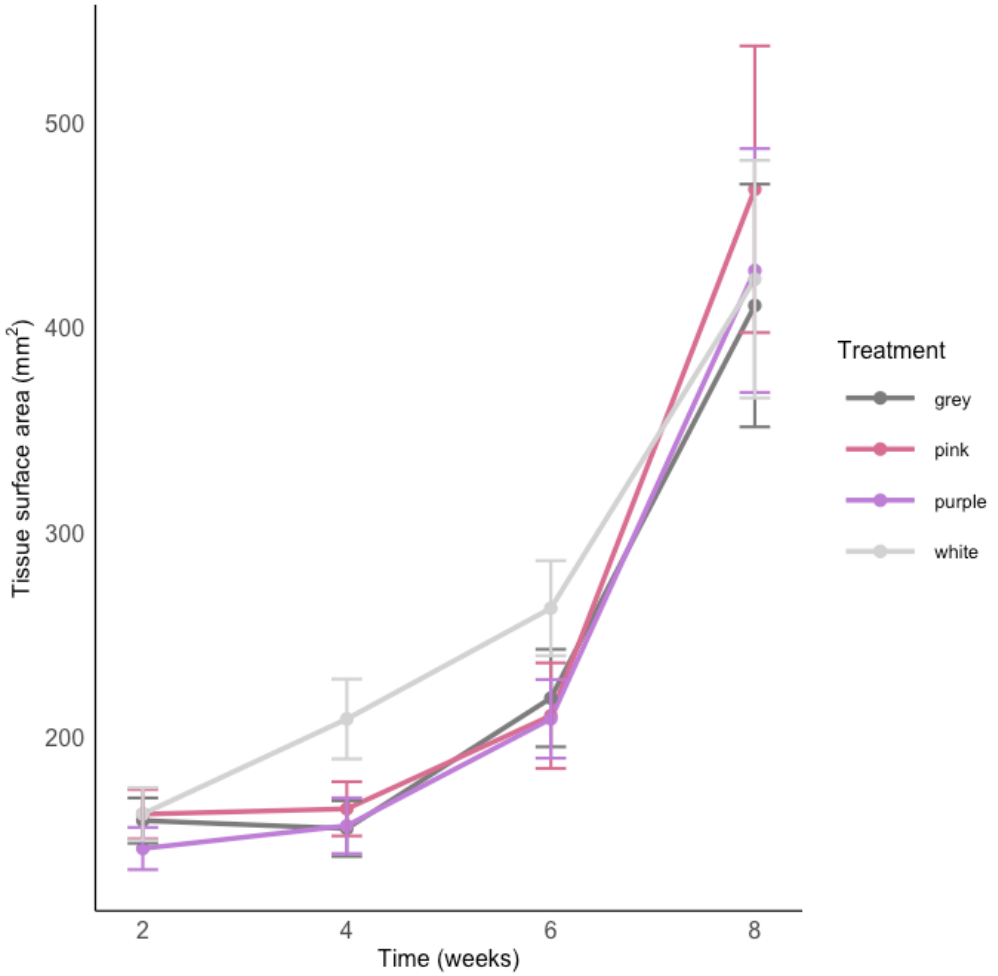

Figure 12. *Orbicella faveolata average (± SE) tissue surface area (mm^2) across the four tile color treatments (white, grey, pink, and purple) measured at 2-, 4-, 6-, and 8-weeks post-settlement.*

Orbicella faveolata showed a significant increase in tissue surface area over time (Estimate = 0.148 ± 0.009, t(193) = 15.87, $p < 0.001$; Fig. 12), but with no significant differences in growth among tile color treatments (all $p > 0.22$).

1.3.5. Choice settlement experiment with *P. clivosa*

Pseudodiploria clivosa settlement was highly variable and was not significantly affected by tile color (all $p > 0.05$; Fig. 13).

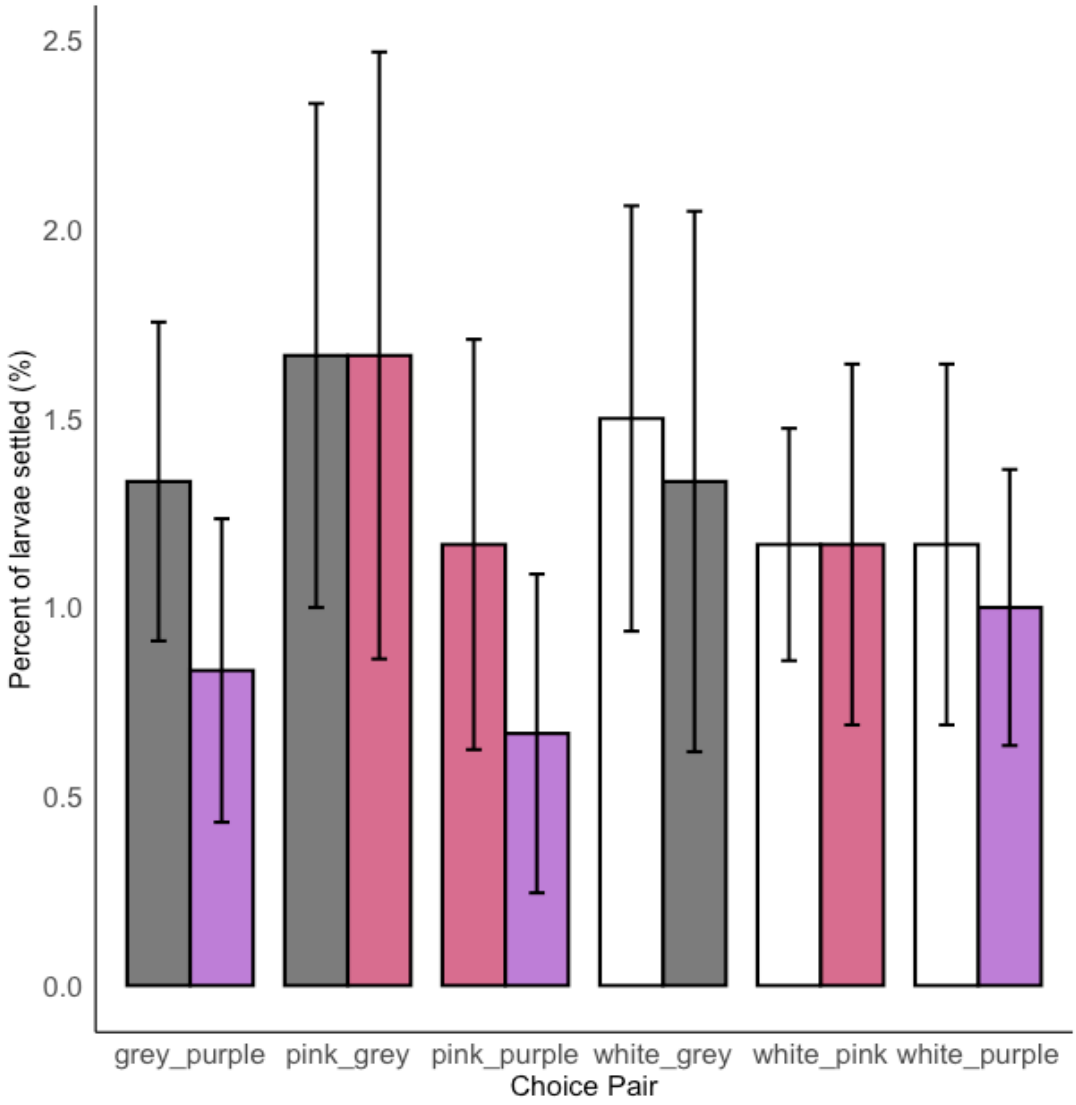

Figure 13. *Average (± SE) percent settlement of Pseudodiploria clivosa recruits within each settlement choice tile color pairing (n = 6).*

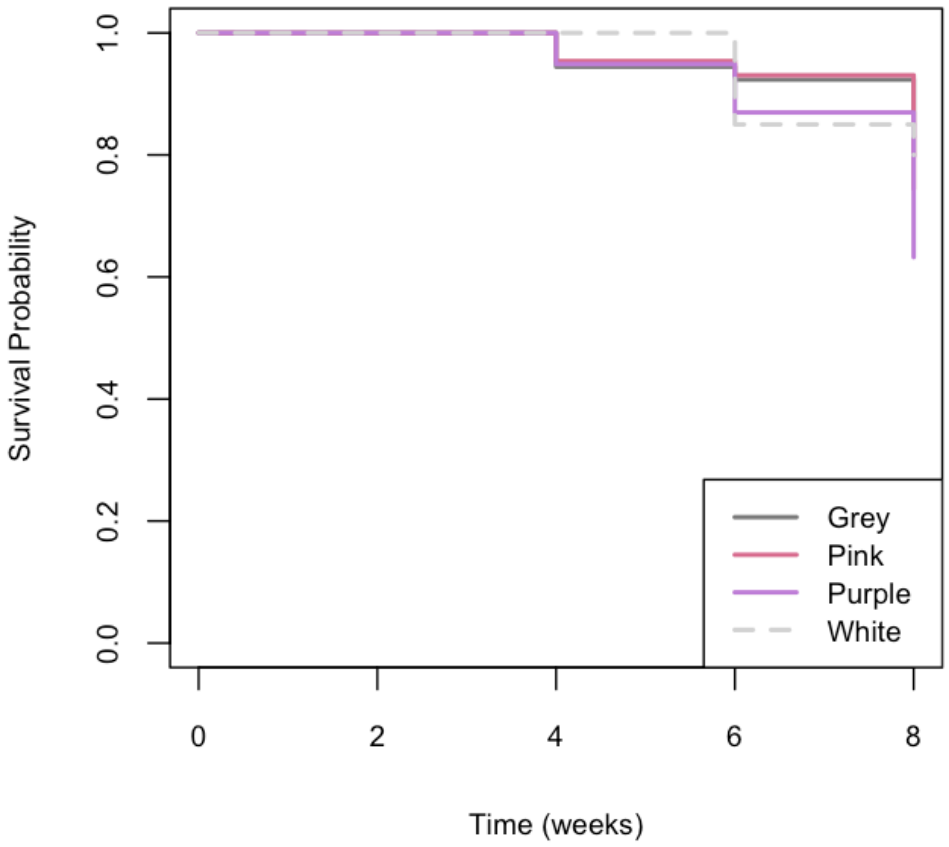

Figure 14. *Probability of survival (Kaplan-Meier survival curves) for Pseudodiploria clivosa over time (2-, 4-, 6-, and 8-weeks post-settlement) by tile color (white, grey, pink, and purple). Lines represent survival probability over time.*

There was no significant effect of tile color treatment on *P. clivosa* recruit survivorship (Mansel-Haenzsel log-rank Survival Analysis, chi-sq = 1.4, df = 3, $p = 0.70$; Fig. 14).

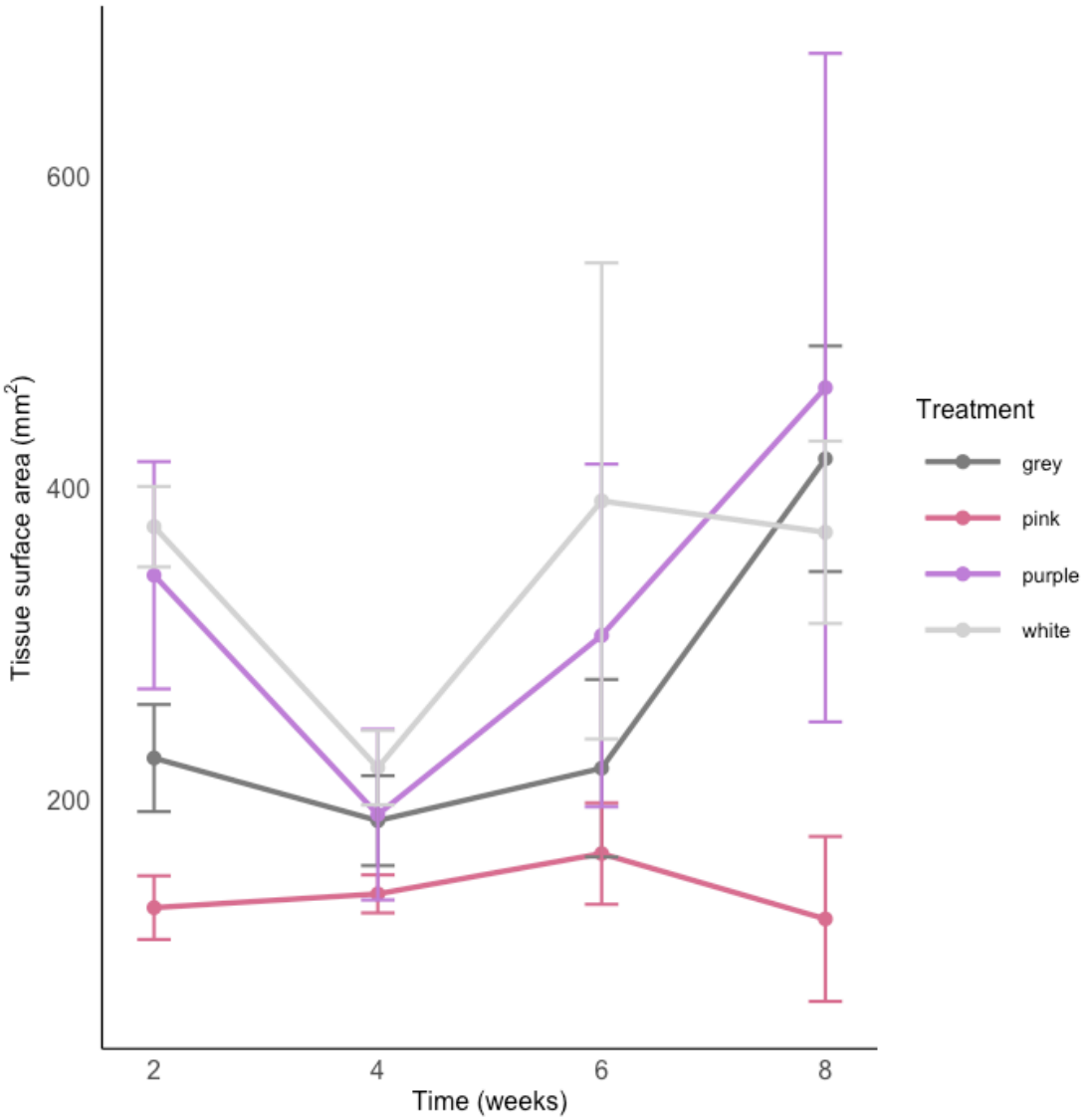

Figure 15. *Pseudodiploria clivosa average (± SE) tissue surface area (mm^2) across the four tile color treatments (white, grey, pink, and purple) measured at 2-, 4-, 6-, and 8-weeks post-settlement.*

There was no significant effect of tile color treatment (all $p > 0.1$) or time ($p = 0.219$) on *P. clivosa* recruit growth (Fig. 15). This is likely due to the high variability in growth among recruits and the cup size and shape making the coral tissue size decrease after 4 weeks. However, a trend of smaller size and less slower growth in pink tile is evident, although not significant.

1.4. Discussion

1.4.1. Spawning and fertilization

The magnitude of *P. clivosa* and *O. faveolata* spawning and quality of gamete bundles (i.e., less buoyant likely from lower lipid content in eggs) was less this year. This could be due to the first spawning season in their new systems, slight differences in Generation 6 Radion light spectrum and lunar tables, and/or the need to increase nutrition due to the large size of these colonies. Additionally, for *P. clivosa* this could be due to an asynchronous spawning event that occurred in early August. On the morning of August 5th, 15 days after the July full moon and outside of the typical spawning window, evidence of spawning was found in the system (i.e., overactive protein skimmer, cloudy tank, lipids on surface). There were no larvae found in the sump, likely because the UV sterilizer killed the sperm and embryos. Although there is no way of knowing, we believe it was a relatively large spawn. We have reverted to the Lunar Simulator Modules (LSM; Neptune Systems) instead of relying on the lunar cycle within the Gen6 Radion lights. We have also tripled the amount of food that we feed each tank in the hope that increased nutrition will lead to a higher magnitude in spawning and higher quality gametes.

1.4.2. Sperm Morphology and Motility

We have successfully assessed sperm morphology in two species, *O. faveolata* and *P. clivosa.* Longer tail sizes between species and between individuals within a species may indicate the ability to swim and fertilize eggs faster. *Orbicella faveolata* is historically found in high densities. Based on fertilization models, the larger head and longer tail size is indicative of a dense population and synchronous gamete release where sperm are under selection for immense competition. *Pseudodiploria clivosa*, on the other hand, are found in less dense populations therefore sperm is likely more limited; therefore, sperm longevity is more likely selected for this species. This will need to be further examined with the new CASA software that will allow us to accurately measure spermvelocity. Similarly, differences in size between normal and abnormal sperm may influence motility and the ability to successfully fertilize eggs. This highlights the need to conduct specific crosses during fertilization, rather than utilizing batch fertilization, to balance the need for high fertilization with the importance of having a diverse parentage in the offspring. While we were unable to record sperm velocity during this spawning season, we are confident that with our improved methodologies, valuable partnerships, and new CASA software, we will record this metric to better understand how sperm fitness varies across individuals and between species to maximize our fertilization potential during future spawning events.

1.4.3. Larvae rearing and settlement

While the new larval system worked well for *Orbicella faveolata*, improvements still need to be made. Due to the flat bottoms of the bins, water remained stagnant at the bottom and only flowed on the surface, which may have contributed to a die-off at 5 days

post-fertilization. To remedy this a second tube was added that reached the bottom of the bin to ensure water would circulate throughout the entire bin. Overall, *O. faveolata* seemed to survive better than *P. clivosa* within this system, which is not surprising given *O. faveolata* larvae prefer lower to no water flow.

We will add a drainage system for each individual bin to aid in condensing the coral larvae. In the future, we will continue to use the larval cones, as well as this new system.

1.4.4. No choice and choice settlement experiments

No choice experiments indicated that purple tiles provided a simple and effective way to upscale *O. faveolata* recruit success. While pink tiles had the highest survivorship probabilities, they also had the lowest settlement success. Purple tiles exhibited equivalent settlement success to white and grey tiles but had significantly higher survivorship probabilities.

In choice experiments*, P. clivosa* recruits showed no preference, survivorship, or growth differences among tile colors. However, overall, they showed lower settlement, survival, and growth compared to previous years, possibly due to changes to broodstock environment, larvae rearing, or broodstock nutrition.

2. PROBIOTIC DOSING OF EARLY LIFE HISTORY STAGES

2.1. Overview

The use of probiotics is an understudied area for coral biology, with a particular focus on how probiotics can enhance coral reproduction, survival, and growth at the earliest life history stages. Collaborating with Dr. Blake Ushijima, the Fogarty lab conducted follow-up experiments to determine whether dosing *P. clivosa* larvae and recruits with promising probiotic isolates tested in 2023 can lead to enhanced survival and growth. In 2022, three isolate mixtures (15, 17, 19) were identified as the most promising probiotic candidates, while in 2023 several single strain putative probiotics for *P. clivosa* were identified. This year, we re-tested the seven most promising individual strains, and two mixtures, to make a final selection and recommendation on a strain, or combination of strains, for use in land-based propagation. Recruits were reared until six months of age, and growth and survivorship were tracked over a 20-week follow-up screening experiment.

2.2. Methods

We dosed *P. clivosa* larvae in glass jars daily over the course of 3 days post-fertilization. Based on results from our previous pilot and screening projects, we used 9 probiotic treatments (inoculants) and 2 controls. Neither control received a probiotic treatment; one control was used for gauging water quality, so a non-dosed, disturbed control and a non-dosed, undisturbed control. The experimental design planned for 75 larvae per jar for all treatments and controls in a decuple, totaling 8,250 larvae distributed across 110 jars. Due to time limitations associated with larval counts, we reduced the number of replicates from 10 to 6, resulting in us inoculating 4,500 larvae among 60 jars. After approximately 24 hours following a successful spawn of our adult *P. clivosa* broodstock, larvae were removed from larval bins and concentrated in 3.8L pitchers before transferring into smaller bowls for counting and placing in jars with transfer pipettes (99 mL of filtered seawater in each jar). The larvae were dosed with 1 mL of the probiotic treatment and subsequently placed in a randomly assigned 37.85 L tank used as a water bath to maintain temperature. Larvae were rinsed with filtered seawater the following night, dosed with the appropriate treatment following the rinse, and jars were replaced in their assigned tanks.

Initial scoring of our adult broodstock for usable *P. clivosa* recruits on settlement tiles occurred on days 13–15 post-spawn (September 9–11 2024). Settlement tiles were reassessed, and baseline photographs of recruits were completed on days 21–23 post-spawn (September 17–19). Treatments included 9 different probiotic consortia and a control receiving no probiotic dosing, each of which contains 24 recruits and 8 replicates per treatment, totaling 240 recruits distributed across 80 tiles. Each of the 8 racks in the experimental system holds one tile from each treatment and the control, representing individual replicates. Of the 9 treatments, 7 were individual bacterial strains (isolates), and 2 were mixtures of 2–3 isolates. The isolates and mixtures of isolates chosen as

treatments showed some promise for enhanced survival and/or growth in our previous 2021 pilot project and our subsequent 2022–23 and 2023–24 screening projects. Like the 2023–24 probiotic experiment, weekly inoculations of *P. clivosa* recruits were conducted in weeks 0–4, followed by an inoculation occurring on week 8, and a final inoculation on week 16, for a total of 7 inoculations (weeks 3–7,11, and 15 post-spawn, respectively).

Tiles were placed in individual jars for inoculations for 24 hours and subsequently rinsed with FSW before being placed back into the raceway. Recruit care and survival counts were conducted weekly until the experimental period concluded in the second week of February 2025. Similar to the 2023–24 screening project, photographs for recruit growth measurements were taken during experimental weeks 0, 8, 12, 16, and 20 (weeks 3, 11, 15, 19, and 22 post-spawn respectively).

Growth quantification was conducted with AI-assisted image analysis in combination with manual tracing (using Olympus CellSens software) to determine recruit surface area. Furthermore, samples (including surviving recruits, tile fragments that supported recruits throughout the experiment, and water from the experimental raceway) were collected and preserved for future microbiome analysis. All samples were preserved in cryovial tubes containing DNA/RNA Shield and stored at –80 °C until DNA extraction occurred. Partial sequencing was used to assess potential differences in microbial community composition across the treatments and the control.

Larval survival data was collected as count data over 3 days. A negative binomial generalized linear mixed model (GLMM) was used to assess larval survival with day (time), treatment, and their interaction included as fixed effects, and jars nested within racks included as random effects.

Kaplan-Meier survival curves were generated to compare recruit survival among treatments, and differences in survival distributions were assessed using a log-rank analysis. A binomial GLMM was used for predicting recruit proportion survival using a logit link function. This models the number of “successes” (alive recruits) and “failures” (dead recruits) as a binomial response. The model includes week and treatment as fixed effects, while rack was included as a random effect to account for variation among replications.

Coral recruit growth was analyzed using a GLMM to evaluate the effects of treatment, time, and initial recruit size on recruit surface area. The response variable was log-transformed to improve normality and reduce right skew. A Pearson’s correlation test revealed a moderate, statistically significant positive relationship between log-transformed initial recruit size and final recruit size ($r = 0.37$, $p < 0.001$), indicating that larger recruits at the start of the experiment tended to be larger at the end of the experiment. Therefore, log-transformed initial size was included as a covariate in the

model. Fixed effects included week (time), treatment, and their interaction, as well as the interaction between week and initial size to account for size-dependent growth. Random effects were included for tile nested within rack to account for non-independence among coral recruits sharing the same experimental surfaces.

2.3. Results

2.3.1. Survival

By the end of the larval dosing experiment on day 3, the mean proportion of larvae surviving across all treatments ranged from about 23% (PsH 17-2 and PsH 17-5) to 41% (G 17-C) (Fig. 16).

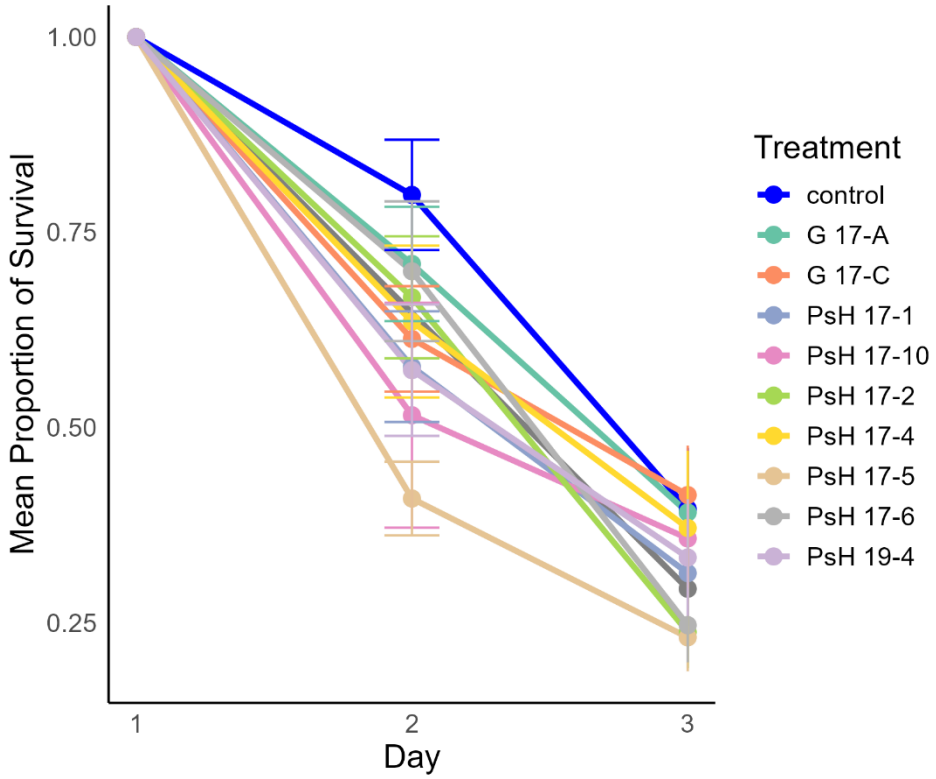

Figure 16. *Average proportion (± SE) of surviving Pseudodiploria clivosa larvae for each day, by treatment (n = 6). Control is represented by the blue line. NB: bacterial consortia G 17-A was missing larval count data from one jar for day 2 (i.e., n = 5).*

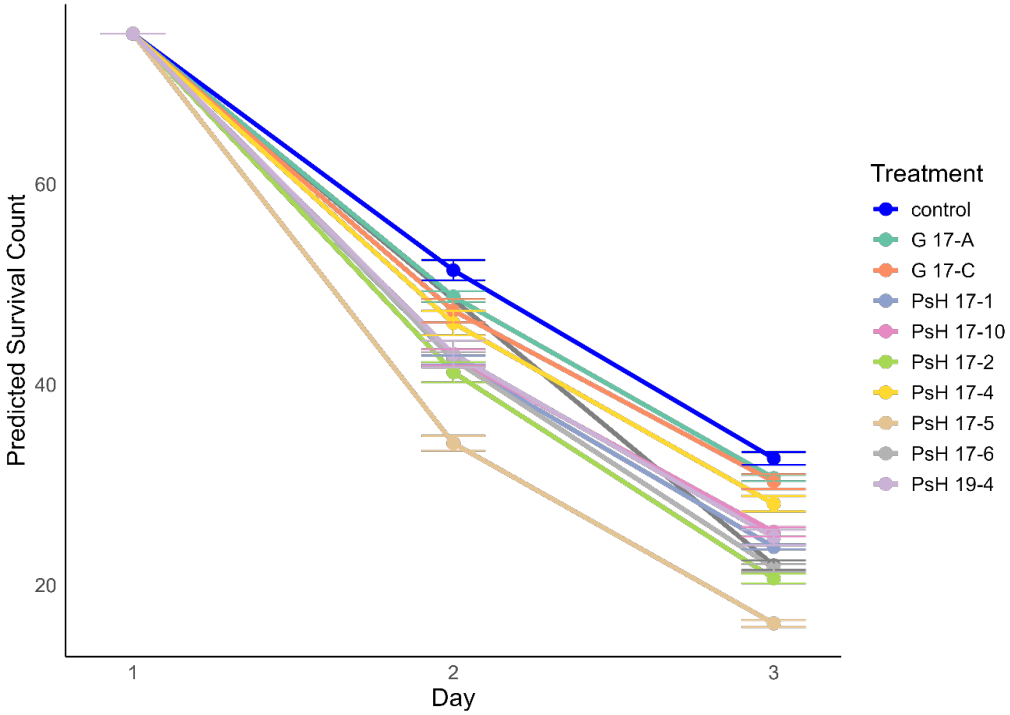

Figure 17. *Model-based predictions of larval survival across treatments over three days using a negative binomial generalized model. Fixed effects were day and treatment and random effects were jar nested within tank. Each line represents the mean predicted survival for a treatment with error bars indicating standard deviations. Control is designated as a blue line. Treatments PsH 17-2 and PsH 17-5 exhibited steeper declines, consistent with observed trends.*

Time had a strong effect on survival, with larval counts declining significantly across days (Estimate = -0.454, $p < 0.0001$). Most treatments did not demonstrate significant impacts on survival independently. Strains PsH 17-2 (Estimate = -0.238, $p = 0.0045$) and PsH 17-5 (Estimate = -0.292, $p = 0.013$) showed significant interactions with time, indicating a faster decline in counts among larvae inoculated with these treatments (Fig. 17).

For recruit survival, log-rank analysis revealed no statistically significant differences among treatments (chi-sq = 11.2, df = 9, $p = 0.30$; Fig. 18). Although not statistically significant, some treatments showed important biological trends. For example, recruits inoculated with strain PsH 17-2 experienced fewer fatalities than were expected by the analysis (3 observed vs. 7.03 expected). However, recruits inoculated with strains PsH 17-5 and PsH 19-4 experienced more fatalities than were expected by the analysis (10 observed vs. 5.81 and 6.05 expected, respectively). In terms of absolute differences in survival rates for recruits, treatment strain PsH 17-2 demonstrated a 13% increase in survival relative to the control (88% vs. 75% survival, respectively; Fig. 19), consistent

with findings observed in the 2023–24 project. Three additional treatments (strains PsH 17-1, PsH 17-6, and consortia G 17-A) each demonstrated a 4% increase in survival compared to the control. Again, these treatments also exhibited increased survival in the previous year's probiotic study. Conversely, three treatments (strains PsH 17-5, PsH 17-10, and PsH 19-4) each demonstrated decreased survival compared to the control (58%, 63%, and 58% vs. 75% survival, respectively). Notably, while PsH 17-5 also showed lower survival in the 2023–24 study, it was associated with enhanced growth relative to the control suggesting potential trade-offs between growth and survival outcomes.

There was a significant decline in survival over time across all treatments (estimate = -0.123, $p < 0.001$; Fig. 20). Four probiotic treatments (PsH 17-2, PsH 17-1, PsH 17-6, and G 17-A) significantly increased the odds of survival relative to the control while PsH 17-5 showed a negative effect on survival (odds ratio = 0.70, estimated survival = 95.1%, $p = 0.037$; Table 3, Fig. 20). The control, which received no probiotic treatment, had an estimated survival probability of 94.0% at the beginning of the experiment. The control served as the reference level in the model, with all probiotic treatment effects expressed relative to this baseline. Notably, PsH 17-2 had the strongest positive effect (odds ratio = 3.95, estimated survival = 98.7%, $p < 0.001$), followed by PsH 17-1 (odds ratio = 2.68, estimated survival = 98.1%, $p < 0.001$), PsH 17-6 (odds ratio = 2.50, estimated survival = 98.0%, $p < 0.001$), and G 17-A (odds ratio = 2.33, estimated survival = 97.9%, $p < 0.001$). PsH 17-6 initially exhibited one of the highest survival rates with no early mortality, but its benefits diminished over time (Fig. 20).

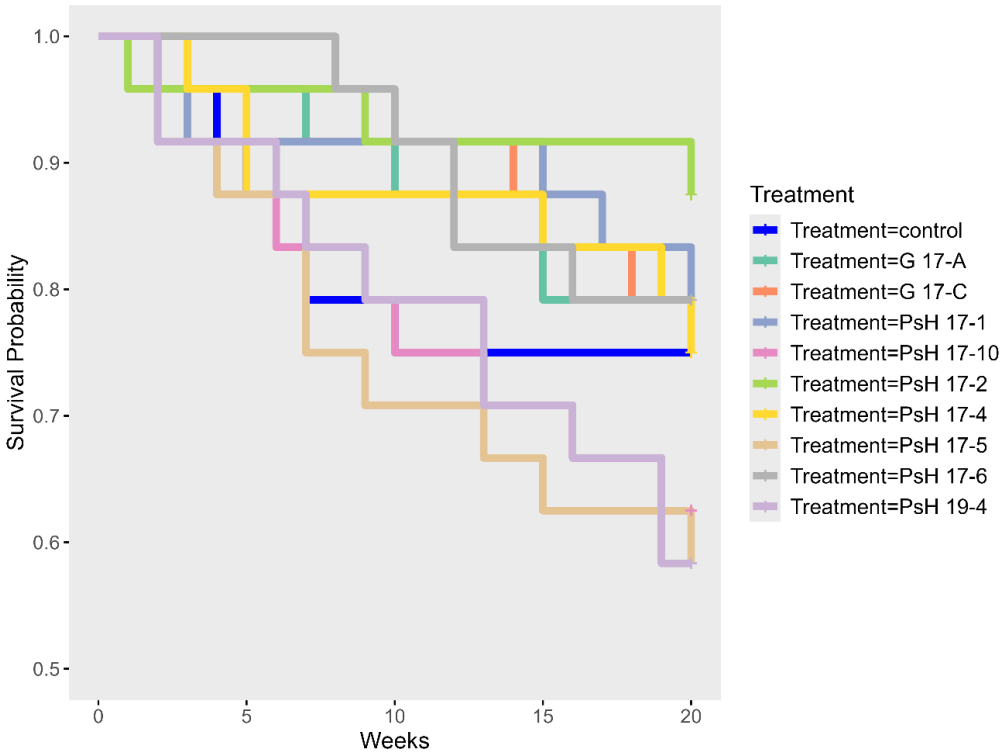

Figure 18. *Pseudodiploria clivosa recruit survival over the 20-week experiment. A log-rank analysis revealed no significant differences (chi-sq= 11.2, df = 9, p = 0.30). The control is designated by the blue line.*

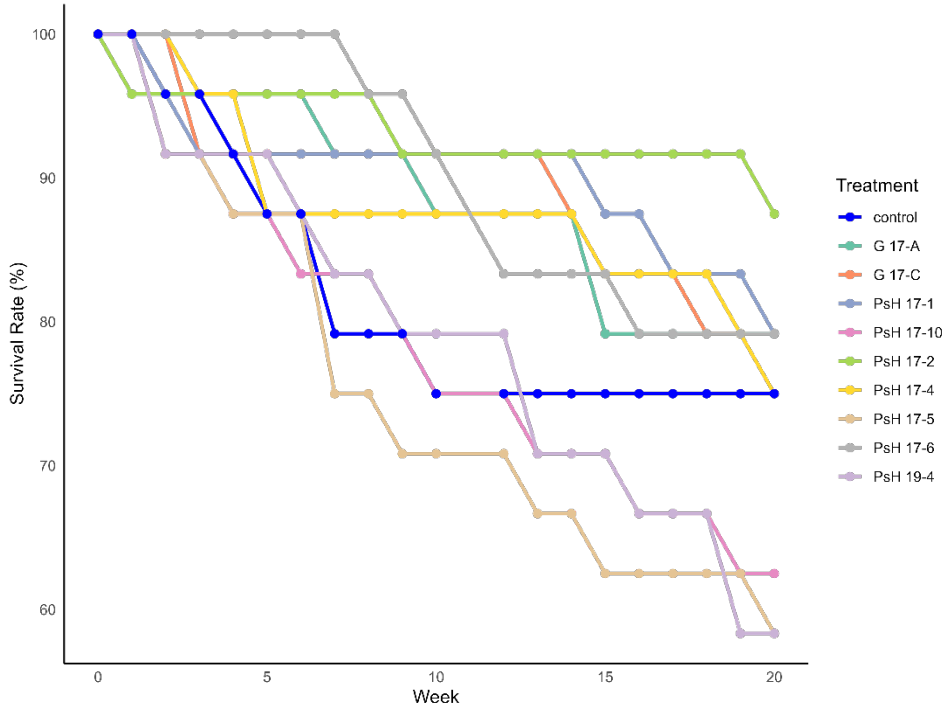

Figure 19. *Survival rates (%) for recruits across all treatments and week.*

Table 3. *A binomial generalized linear mixed model estimated odds ratios and survival probabilities for each probiotic treatment relative to the control at the start of the experiment. PsH 17-2 exhibited the highest predicted survival (odds ratio = 3.95, estimated survival = 98.7%) with a nearly 4-fold increased odds of survival relative to control (odds ratio = 1, estimated survival = 94.0%). Treatments PsH 17-1, PsH 17-6, and G 17-A also performed significantly better than the control ($p < 0.05$), while PsH 17-5 showed significantly lower survival (odds ratio = 0.70, 95.1%, $p = 0.037$).*

Treatment	Odds Ratio	Estimated Survival %	*p*-value
Control	1.0	95.2	< 2e-16
G 17-A	2.33	97.9	2.54e-05
G 17-C	2.11	97.6	0.000227
PsH 17-1	2.68	98.1	2.22e-06
PsH 17-10	1.03	95.3	0.868781
PsH 17-2	3.95	98.7	2.94e-09
PsH 17-4	1.88	97.4	0.001371
PsH 17-5	0.70	93.2	0.036568
PsH 17-6	2.5	98.0	1.04e-05
PsH 19-4	0.73	93.5	0.080614

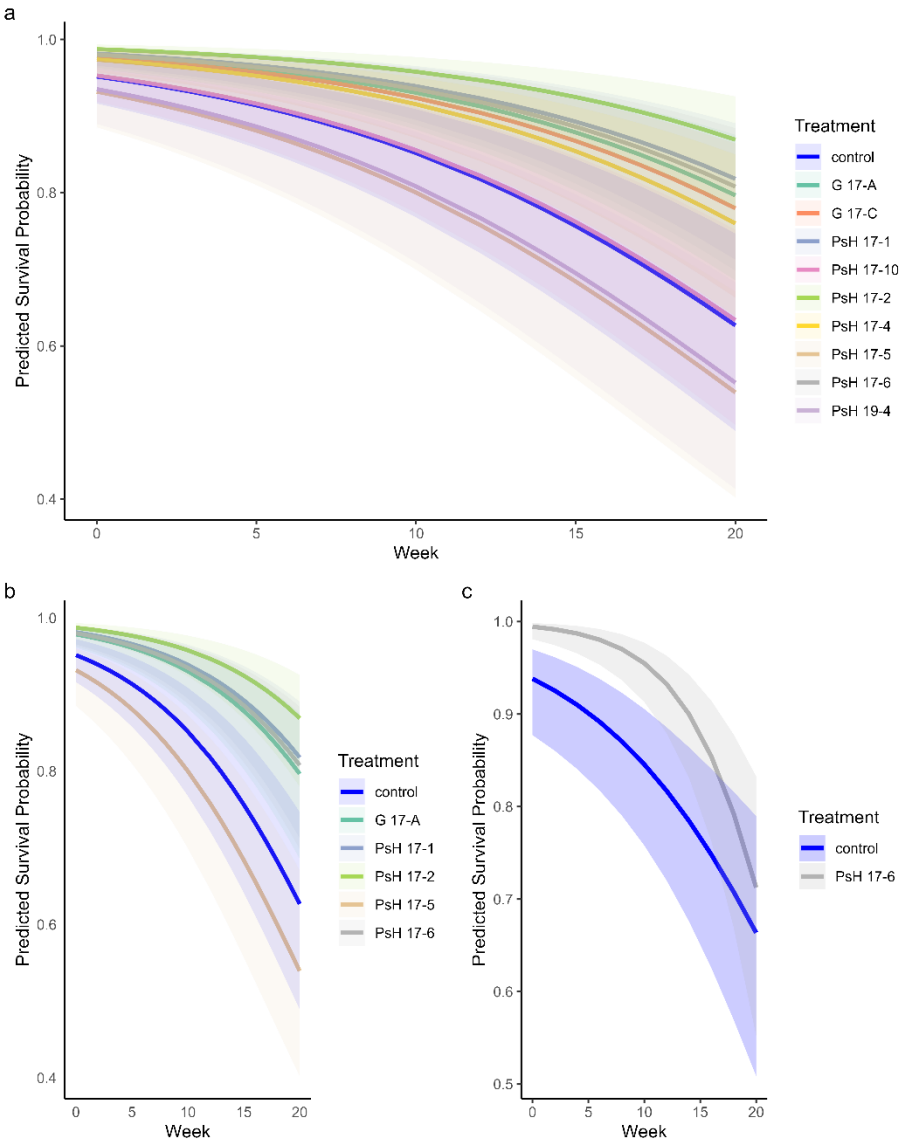

Figure 20. *Model-predicted survival trajectories of Pseudodiploria clivosa recruits based on a binomial GLMM with fixed effects for Time and Treatment, and Replicate as a random effect:* ***A)*** *across all probiotic treatments,* ***B)*** *for the four treatments with the highest odds of survival relative to the control (PsH 17-2, PsH 17-1, PsH 17-6, and G 17-A) and the treatment with the lowest odds of survival relative to the control (PsH 17-5), and* ***C)*** *for PsH 17-6 and the control. PsH 17-6 initially exhibited high survival relative to the control. Its survival trajectory exhibited a steeper decline beginning around weeks 10-12. This diminished survival could indicate that the early benefits of PsH 17-6 may not have been sustained throughout the experiment. In each instance lines represent predicted survival probabilities, shaded ribbon areas represent 95% confidence intervals, and the control is shown in blue.*

2.3.2. Growth

Initial recruit size was a strong predictor of final size (Estimate = 0.913, $p < 0.001$). A significant interaction between week and initial size (Estimate = 0.037, $p = 0.0002$) indicated that larger recruits grew faster over time. Two treatments, G 17-A and PsH 17-5 exhibited significantly higher growth rates compared to the control (week × treatment Estimates = 0.042 and 0.036, $p = 0.013$ and 0.039, respectively). The fixed effects of time and treatment explained 66.5% of the variance (marginal R^2), while the full model, including the random effects of tile nested within rack, explained 74.8% (conditional R^2). This indicates that the model explained a large amount of variation in recruit growth. Model-predicted growth trajectories were then generated to show estimated log-transformed (predictions were back-transformed by the model) area across 20 weeks for each treatment group (Fig. 21). Observed growth trajectories followed the same trends as the model-based predictions with treatment G 17-A and PsH 17-5 exhibiting some of the highest growth rates (Fig. 22).

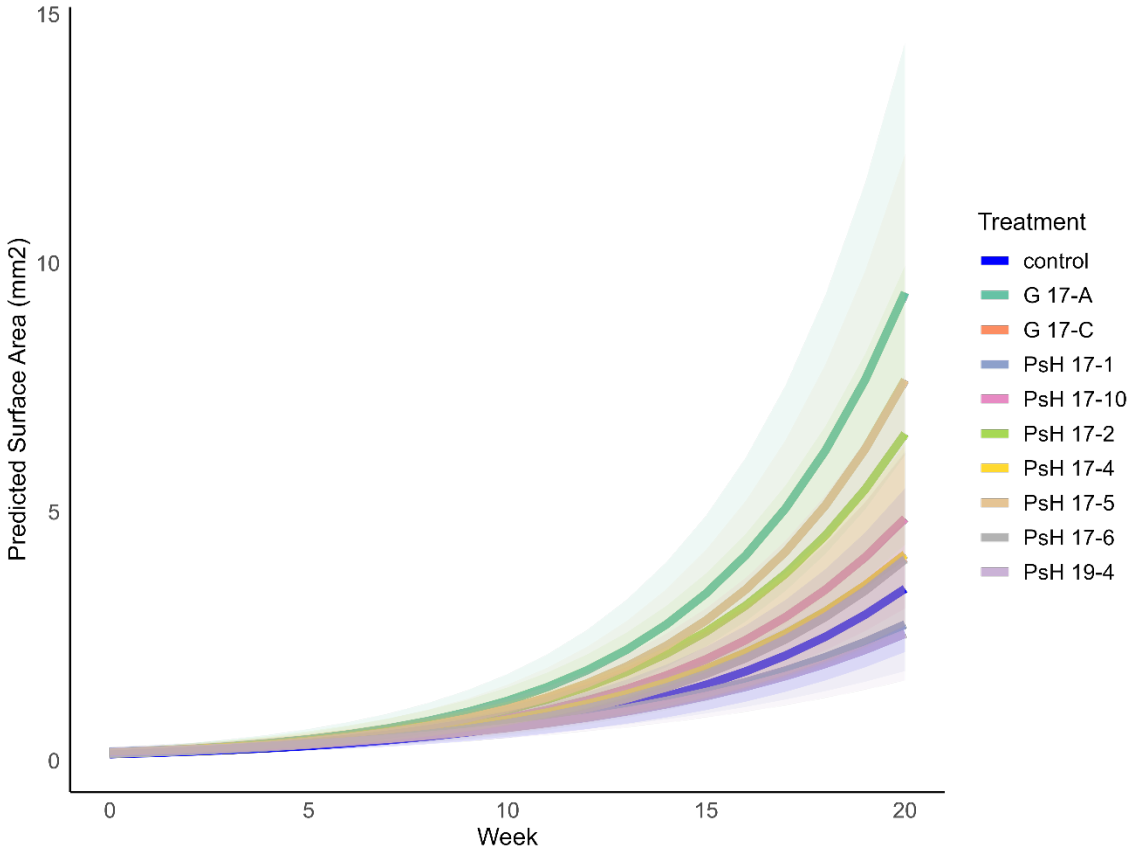

Figure 21. *Model-predicted Pseudodiploria clivosa recruit growth trajectories over 20 weeks for each treatment group. Predictions were generated from a generalized linear mixed model with log-transformed area as the response variable and fixed effects for treatment, time, the log-transformed initial recruit size, and their interactions. Tile nested*

within replicate were included as random effects. Shaded ribbons represent 95% confidence intervals. The control is represented by the blue line.

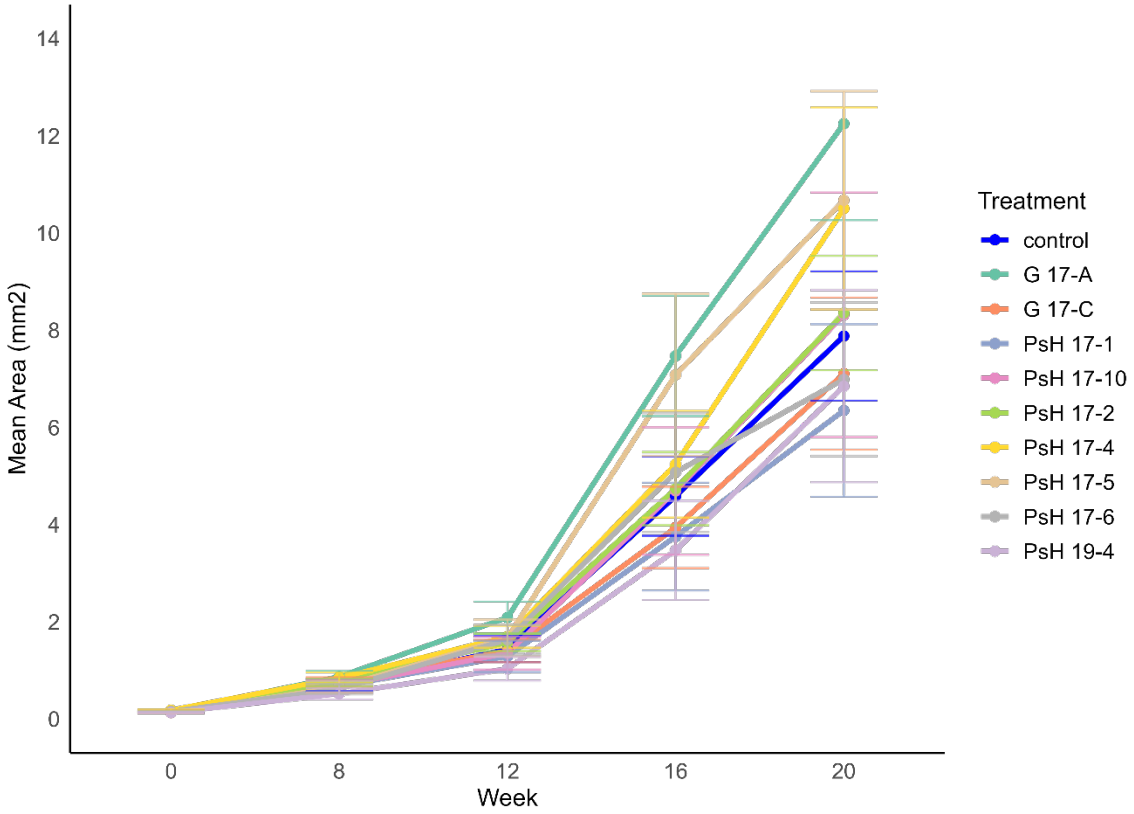

Figure 22. *Mean area (± SE) of Pseudodiploria clivosa recruits within each treatment group at each of 0, 8, 12, 16, and 20-weeks post-settlement. The control is represented by the blue line. Strains PsH 17-2, PsH 17-4, PsH 17-5, and consortia G 17-A demonstrate higher growth compared to control.*

While AI-assisted image analysis is showing strong potential to dramatically reduce the need for manual tracing of recruit photographs, it does not achieve 100% accuracy. As a result, quality assurance and control checks remain essential, and manual tracing is still required for images when AI analysis fails. Therefore, this continues to be a time-intensive component of data processing.

2.3.3. Microbiome composition

Preliminary results suggest that microbiome composition differs between the fragments and the tiles, while composition of fragments which received probiotic doses do not appear to be different from the control (Fig. 23). Additionally, the tank water sample also appears to have a different microbiome composition from all other samples (control fragments, experimental fragments, control tile, and experimental tiles; Fig. 24).

It should be noted, however, that further analysis must be conducted at this time. For example, Fig. 23 includes “Chloroplast” reads, which need to be removed from the dataset prior to statistical analyses.

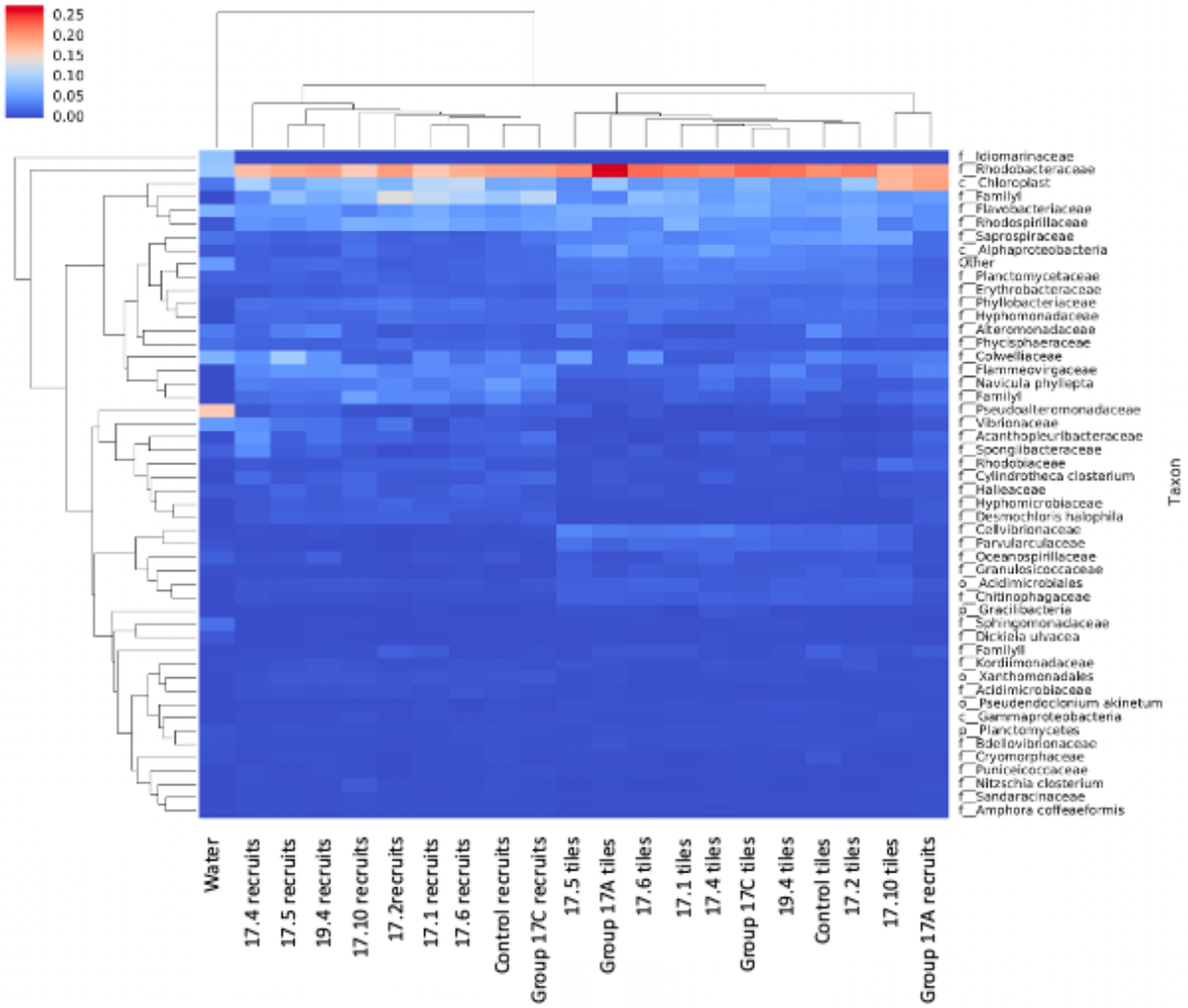

Figure 23. *Heatmap of microbiome composition to family level of control tiles, control recruits, experimental tiles, experimental recruits, and the experimental tank water. Number (i.e., 17.4) corresponds to the PsH strain that the tile or recruit was exposed to during the experiment.*

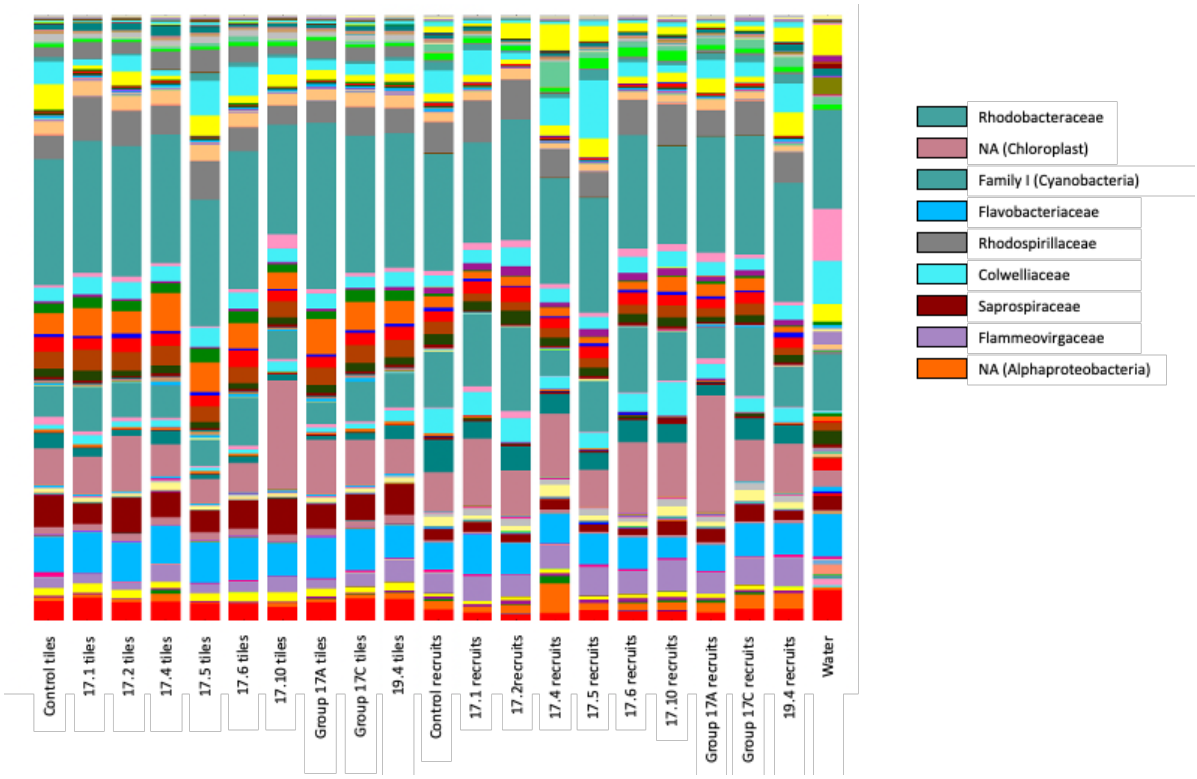

Figure 24. *Microbiome composition to family level of control tiles, control recruits, experimental tiles, experimental recruits, and the experimental tank water. Number (i.e., 17.4) corresponds to the PsH strain that the sample (recruit and corresponding tile) was exposed to during the experiment. NB: only the top 9 (>2.5%) families are shown in the key.*

2.4. Discussion

A similar pattern of enhanced recruit survival was observed again this year for strain PsH 17-2, while strains PsH 17-5 and PsH 19-4 continue to exhibit lower survival compared to the control. However, strain PsH 17-5 does consistently show promise for increased growth. Bacterial mixture G 17-A (formerly G 17-1) demonstrated higher survival in the 2023-24 experiment, but lower growth compared to the control. Interestingly, this year we excluded strain PsH 17-3 from this mixture, and G 17-A demonstrated a significant positive impact on growth, while being slightly less successful for survival. Furthermore, two of the three strains included in G 17-A had positive effects on either survival (PsH 17-2) or growth (PsH 17-5). Interestingly, for larval survival, strains PsH 17-2 and PsH 17-5 demonstrated potential negative effects. This highlights important considerations for our future studies—the potential importance of strain-strain interactions within probiotic mixtures and potential trade-offs associated with survival and growth—underscoring the need for thoughtful strain selection and mixture combinations. For the upcoming 2025 spawning season, we need to continue to further investigate, and upscale, the application

of strain PsH 17-2, as it continues to show promise for enhanced survival, and G 17-A with the same strains from this year to further assess positive impacts on growth. Strain PsH 17-6 initially exhibited one of the highest survival rates and delayed early mortality, but its benefit seemed diminished over time, suggesting that its positive effect may not have been sustained throughout the experiment. Given that PsH 17-6 experienced no mortality longer than any other treatment in this year's experiment, this may also be a viable option to further explore, perhaps involving additional inoculations with this strain. Finally, it is promising that the microbial composition of fragments which received probiotic doses do not appear to be different from the control, as this suggests that the addition does not reduce diversity or the presence of other beneficial bacteria; however, further analysis into the microbiome composition is needed.

3. FLORIDA CORAL SPAWNING PATTERNS

3.1. Overview

Coral spawning is synchronized at multiple time scales (month, day, hour, and even minutes). This synchronization is completed through the perception of multiple environmental cues, namely annual ocean temperature variations, as well as light fluctuations from the lunar cycle and changes in the daily photoperiod. Any shifts in these environmental cues, whether historical or geographical, could therefore disrupt synchronous coral spawning. Asynchronous spawning drastically reduces the chance of fertilization between colonies, preventing coral recruitment and the consequent recovery of Florida's Coral Reef. This project aims to document spawning times for several Florida coral species and identify differences in historical and geographical spawning patterns.

3.2. Methods

Over 1000 spawning observations have been compiled from various sources including peer-reviewed journals, data from NOAA's Coral Health and Monitoring Program Coral ListServer, posts from the Coral Spawning Research Facebook page, and unpublished data contributions from researchers throughout Florida. This thirty-year dataset (1993–2024) represents spawning information for seventeen species, including priority species, *O. faveolata*, *P. clivosa*, *P. strigosa, D. labryrinthiformis,* and *Montastraea cavernosa*. Additionally, through a combination of field and aquaria observations, we have obtained spawning information about lesser understood species, including *Mussa angulosa*, *Mycetophyllia lamarckiana*, and *Eusmilia fastigiata.* However, only analyses for species with sufficient spawning data (i.e., *A. cervicornis, A. palmata,* and *O. faveolata)* have been conducted to determine whether there are historical shifts and/or regional differences in *in situ* spawning (at the scale of days and hour) using a Kruskal Wallis test was used. Similarly, where data was sufficient, differences in spawning times between *in situ,* induced (i.e., in captivity for a full gametogenic cycle under artificial lighting), and ex situ (i.e., temporarily in captivity under natural lighting) data were determined via Kruskal Wallis analyses.

3.3. **Results**

A sufficient number of observations were collected for nine species to determine spawning times (Table 4).

Table 4. *Spawning times for Florida corals based on in situ and ex situ data. * indicates minutes before sunset.*

Species	Spawning Month(s)	DAFM	MAS
Acropora cervicornis	July-September	0-15	30-207
Acropora palmata	July-September	0-15	55-171
Dendrogyra cylindrus	July-August	1-5	54-138
Diploria labyrinthiformis	April-June	9-13	55*-210*
Montastraea cavernosa	July-September	1-8	46*-167
Orbicella annularis	August-September	6-8	185-216
Orbicella faveolata	July-September	5-10	97-260
Pseudodiploria clivosa	August-September	7-10	284-476
Pseudodiploria strigosa	August-September	5-13	86*-18; 97-239

Spawning data spans 23 years (2001–2024) for *A. cervicornis*. Spawning for this species occurred from 0–15 days after the full moon (DAFM), between 30–207 minutes after sunset (MAS). There were significant differences in regional spawning times, at both the DAFM (Fig. 25A; chi-sq = 11.87, df =3, $p < 0.01$) and MAS (Fig. 25B; chi-sq = 11.87, df =3, $p < 0.01$) scale. The Upper Florida Keys spawned significantly earlier in terms of DAFM compared to the Middle Keys ($p < 0.05$), but not significantly earlier than Southeast Florida, Upper and Lower Florida Keys ($p > 0.05$). All other regions did not have significantly different spawning days ($p > 0.05$). Similarly, the Upper Florida Keys spawned significantly earlier in terms of MAS than Southeast Florida (chi-sq = 29.887, df = 2, $p < 0.0001$), but not earlier than the Middle Florida Keys ($p > 0.05$). There is insufficient data from the Middle Florida Keys to assess synchrony at the MAS level.

To assess historical shifts in spawning, observations were placed into bins spanning ~8 years (e.g., 2001–2008, 2009–2017, 2018–2024). There were no significant differences between days (Fig. 25C; chi-sq = 1.7476, df = 2, $p = 0.4174$), nor minutes (Fig. 25D; chi-sq = 1.6203, df = 2, $p = 0.4448$), of spawning. There were no significant differences in the day of spawning based on whether observations were conducted *in situ,* in an induction system, or ex situ (Fig. 26A; chi-sq = 1.6635, df = 2, $p = 0.4353$). However, there was a significant difference in spawning time in MAS depending on observation method (Fig. 26B; chi-sq = 28.679, df = 2, $p < 0.0001$). Specifically, corals observed spawning ex situ spawned significantly later in MAS than corals observed spawning *in situ* ($p < 0.05$).

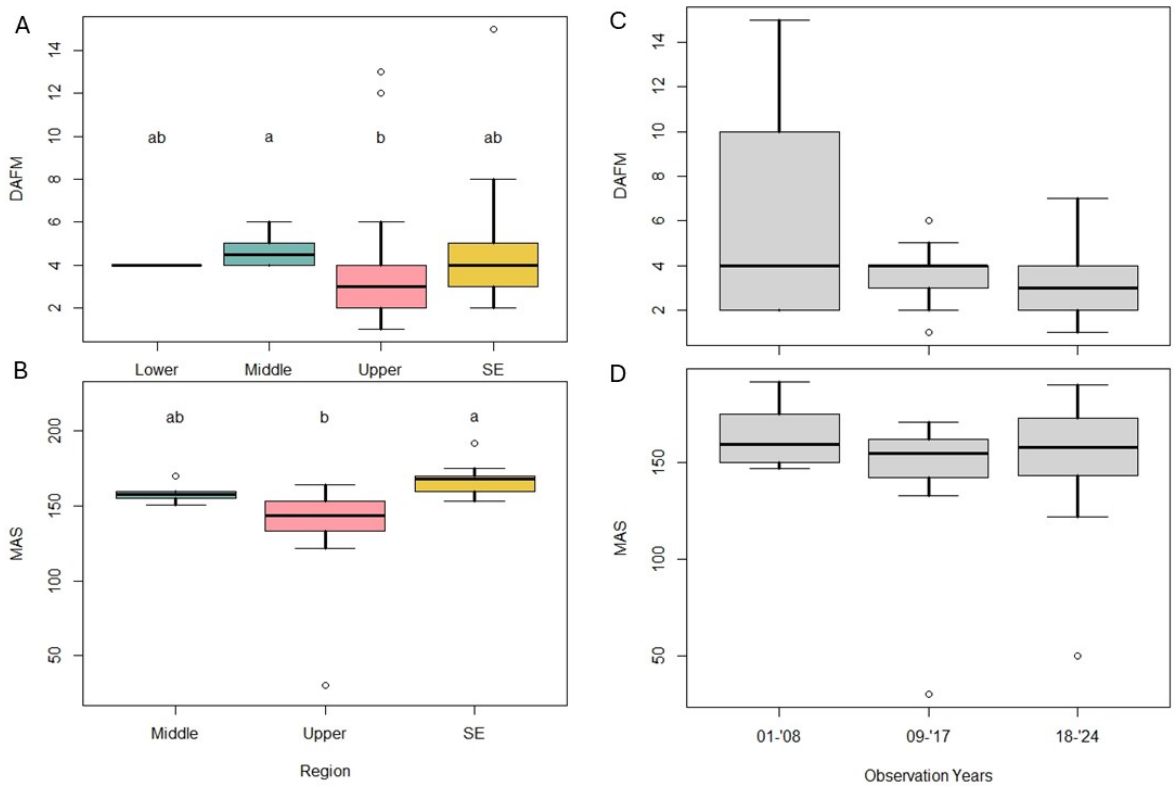

Figure 25. *Regional shifts in spawning times for Acropora cervicornis in A) DAFM and B) MAS. Historical shifts in spawning times for Acropora cervicornis in C) DAFM and D) MAS. Letters indicate statistical significance.*

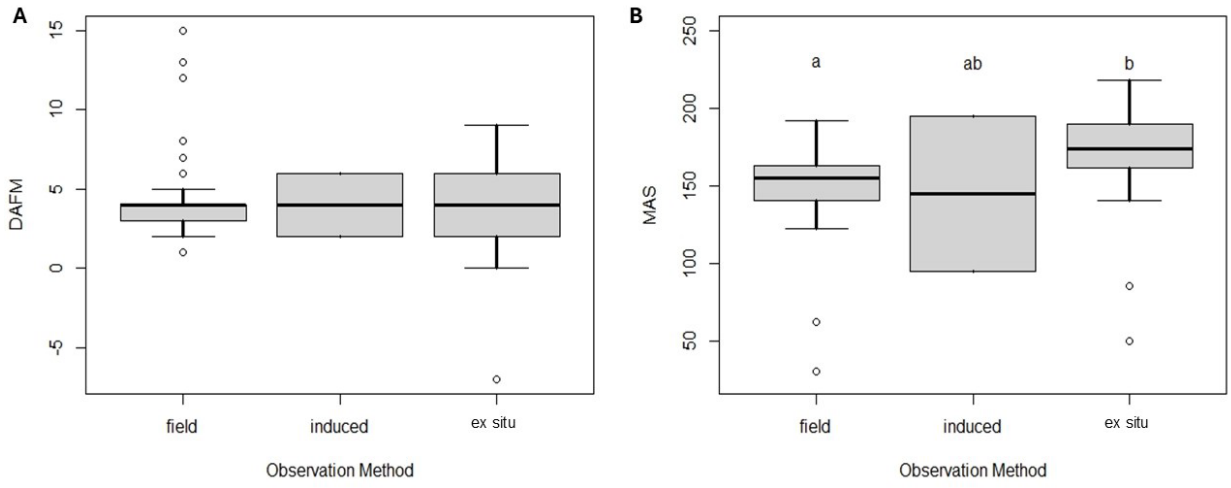

Figure 26. *Acropora cervicornis spawning times do not differ based on observation method at the A) DAFM scale, but shifts in B) MAS can be seen based on the spawning observation method. Letters indicate statistical significance.*

Spawning data spans 28 years (1995–2023) for *A. palmata*. Spawning for this species occurred from 0–12 days after the full moon (DAFM), between 55–171 minutes after sunset (MAS). There were no significant differences in regional spawning times in terms of DAFM (Fig. 27A; chi-sq = 4.1896, df = 2, $p = 0.1231$). However, there were significant differences in spawning in terms of MAS by region (Fig. 27B; chi-sq = 8.6764, df = 2, $p < 0.05$). Similar to patterns observed in *A. cervicornis*, *A. palmata* in the Upper Florida Keys spawned significantly earlier in terms of MAS than Southeast Florida ($p < 0.05$). Additionally, *A. palmata* in the Lower Florida Keys spawned significantly earlier than those in Southeast Florida at the MAS scale ($p < 0.05$). There were no significant differences between the Lower and Upper Keys spawning times in terms of MAS ($p > 0.05$) and there was insufficient data from the Middle Florida Keys to assess synchrony at the MAS level.

To assess historical shifts in spawning, observations were placed into bins spanning ~9 years (e.g., 1995-2004, 2005-2013, 2014-2023). There were significant differences between days (Fig. 27C; chi-sq = 22.945, df = 2; $p < 0.0001$), with spawning occurring closer to the full moon in 2014–2023 than in 1995–2004 and 2005–2013 ($p < 0.05$). However, there were no significant differences between spawning times in minutes after sunset (Fig. 27D; chi-sq = 2.6049, df = 2, $p = 0.2719$), of spawning.

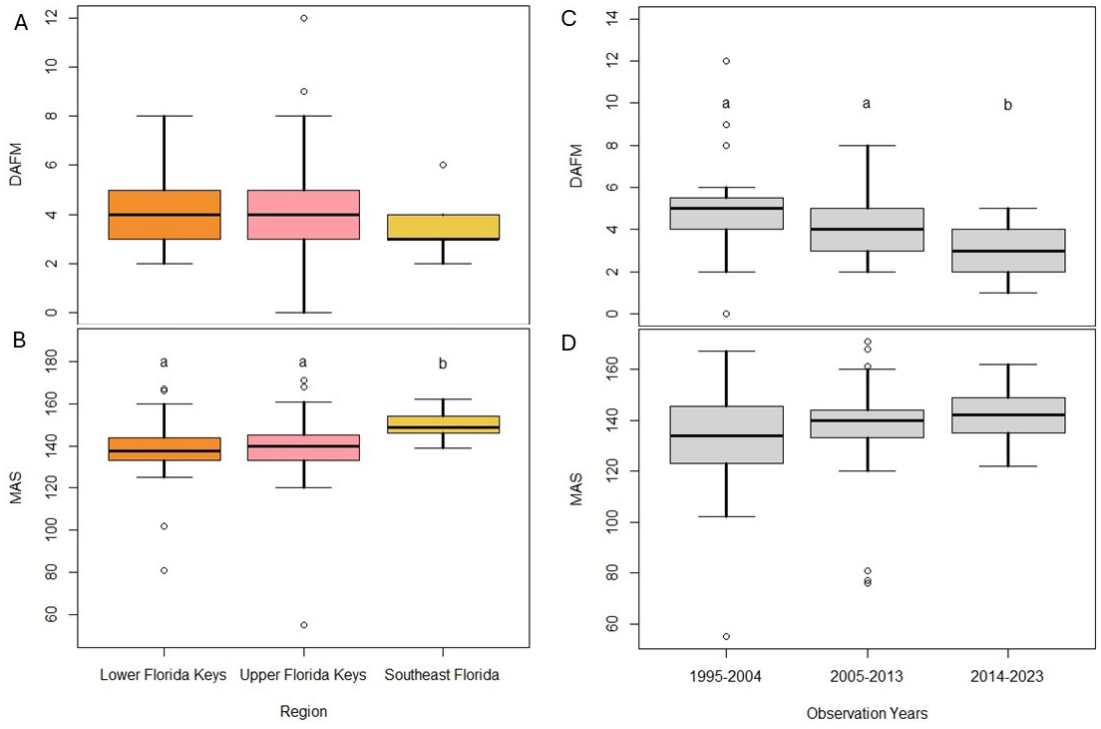

Figure 27. *Regional shifts in spawning times for Acropora palmata in A) DAFM and B) MAS. Historical shifts in spawning times for Acropora palmata in C) DAFM and D) MAS. Letters indicate statistical significance.*

Spawning data spans 31 years (1993–2024) for *O. faveolata*. Spawning for this species occurred from 5–10 DAFM, between 97–260 MAS. There were significant differences in regional spawning times, at both the DAFM and MAS scale. The Upper Florida Keys spawned significantly earlier in terms of DAFM compared to the Middle Keys (Fig. 28A; chi-sq = 10.152, df = 3, $p < 0.05$), but not significantly earlier than Southeast Florida ($p > 0.05$), Upper ($p > 0.05$) and Lower Florida Keys ($p > 0.05$). All other regions did not have significantly different spawning days ($p > 0.05$). There were no significant differences in spawning time in terms of MAS between Southeast Florida and the Upper Florida Keys (Fig. 28B; chi-sq = 2.0805, df = 1, $p = 0.1492$). There was insufficient data from the Middle and Lower Florida Keys to assess synchrony at the MAS level.

To assess historical shifts in spawning, observations were placed into bins spanning 10 years (e.g., 1993–2004, 2006–2014, 2015–2024). While there were no significant differences between days of spawning (Fig. 28C; chi-sq = 0.59823, df = 2, $p = 0.7415$), there were significant differences between the minutes of spawning (Fig. 28D; chi-sq = 10.978, df = 2, $p < 0.01$). Specifically, corals between 2015–2024 spawned significantly later in the evening than corals that spawned between 1993–2004 ($p < 0.05$). There were no significant differences in spawning minutes between 1993–2004 and 2006–2014 ($p > 0.05$), nor between 2006–2014 and 2015–2024 ($p > 0.05$). There were significant differences in the day of spawning based on whether observations were conducted *in situ,* in an induction system, or ex situ (Fig. 29A; chi-sq = 28.173, df = 1, $p < 0.0001$), with *in situ* corals spawning closer to the full moon than corals in induction systems ($p < 0.05$). Similarly, there was a significant difference in spawning time in MAS depending on observation method (Fig. 29B; chi-sq = 5.6117, df = 1, $p < 0.05$). Specifically, corals observed spawning *in situ* corals spawned earlier in the evening than corals in induction systems ($p < 0.05$).

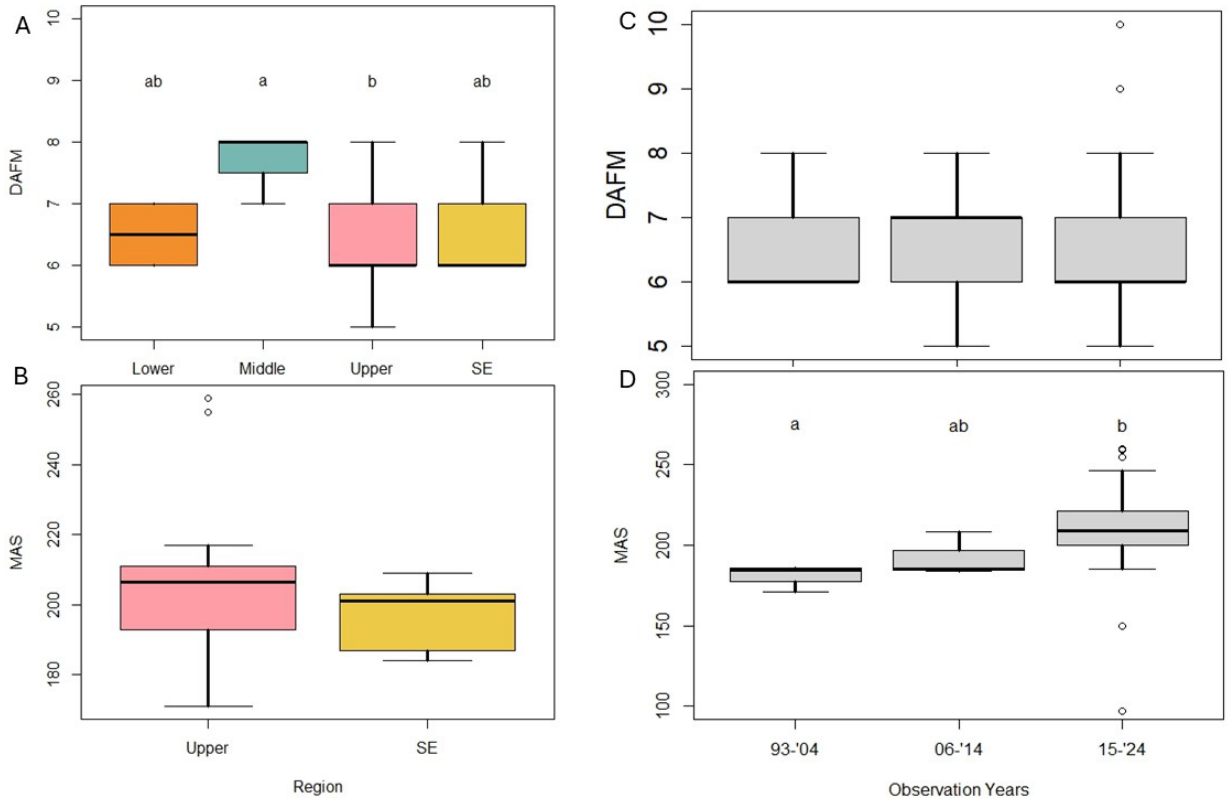

Figure 28. *Regional shifts in spawning times for Orbicella faveolata in A) DAFM and B) MAS. Historical shifts in spawning times for Orbicella faveolata in C) DAFM and D) MAS. Letters indicate statistical significance.*

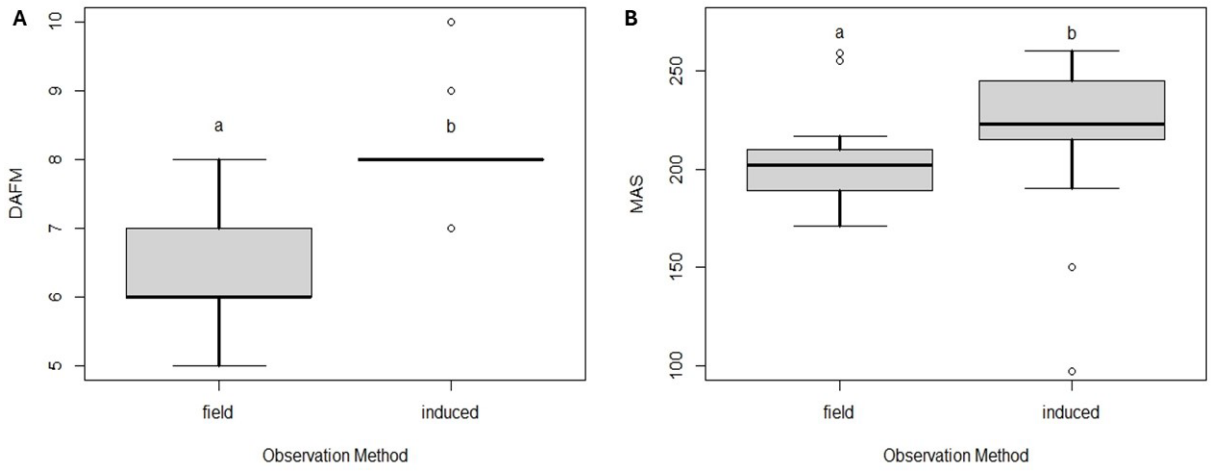

Figure 29. *Orbicella faveolata spawning times differ based on observation method at the A) DAFM and B) MAS time scales. Letters indicate statistical significance.*

3.4. Discussion

Historical shifts in the timing of spawning at both the day and minute scale highlight the importance of long-term monitoring to better understand how environmental changes influence the synchrony of coral spawning. Understanding these changes can help scientists and restoration practitioners to better prepare for monitoring *in situ* to aid in assisted fertilization. Regional differences in spawning times also indicate that micro-environmental factors may influence the timing of coral reproduction and future work should delve into understanding regional differences in temperature and light availability may impact coral reproduction. Regional asynchrony in spawning times also highlights the importance of spawning induction systems. Collecting broodstock throughout Florida's Coral Reef would maximize the chances of fertilization success between genetically diverse parents that would not normally create offspring in the wild due to both temporal and geographic restraints. Differences in spawning times based on observation methods indicate that key environmental cues, namely light, play a large role in the synchrony of coral spawning. Previous studies have shown that ex situ coral spawning occurs later in the evening than *in situ,* likely due to artificial night light pollution. Furthermore, while induction systems can reliably induce gametogenesis and spawn corals in captivity, it is not perfectly synchronous with spawning times *in situ*. This may indicate improvements in the delivery of environmental cues, either through more precise programming or through additional fine-scale environmental factors, are necessary to truly mimic *in situ* conditions.

There was a limited amount of in situ spawning data in 2024, likely as a latent effect of the 2023 bleaching event. Furthermore, there is limited ex situ spawning data for many species. Because of these limitations, we were unable to conduct analyses comparing the spawning observation methods for many species. As corals in the wild recover from the 2023 bleaching event and ex situ spawning systems mature and expand to more diverse species, we anticipate having an adequate data set to compare in situ vs. ex situ spawning times at both the day and hour levels of spawning synchrony.